Evaluation of Miniaturized Mixer and Integrated Optical Components for Cell Sorting

By

Shuwen Wang

A thesis
presented to the University of Waterloo
in fulfillment of the
thesis requirement for the degree of
Master of Applied Science
in
Mechanical Engineering

Waterloo, Ontario, Canada, 2008

Author’s Declaration

I hereby declare that I am the sole author of this thesis. This is a true copy of the thesis, including any required final revisions, as accepted by my examiners.

I understand that my thesis may be made electronically available to the public.

Abstract

Conventional cell cytometers are often bulky and thus not convenient for bio-medical analysis where portable devices are desired. They also suffer from the drawback of high cost due to the complicated and expensive optical detection system involved. Therefore miniaturizing conventional cell cytometer is highly demanded as it offers an opportunity to transform the conventional bulky systems to more cost-efficient and portable microfluidic cell sorting devices. In addition to the advantages reduced cost and enhanced portability, microfluidic cell sorting devices require only a tiny amount of sample for analysis. In this thesis, one common microfluidic cell sorting device is developed using similar conventional functions and concepts but different sorting method. Unlike most of the conventional cell cytometers in which an electrical field or magnetic field is employed to deflect the charged target cells to the collecting container, microfluidic cell sorting devices use the fluid flow to control the movement of the targeted cells to the collecting reservoir. By using an electroosmitic pump, the response time of the flow switch is significantly lowered, leading to a much higher sorting efficiency.

Despite the advantages of microfluidic cell sorting devices, there are some issues need to be addressed before realization of such devices. For example, more studies are required on the successful integration of the optical elements in the devices. In microfluidic, the transport phenomena is also different from that in macroscopic. Unlike that in macroscopic, surface forces are important in microfluidics. They result in pressure-induced flow which gives the parabolic profile of the velocity along the channel. Also, a plug-like velocity which is generated by the electoosmitic flow is required for the more controllable and accurate detection. To suppress the pressure-driven flow, hydro-resistance elements (Shallow channel network) are implemented on the microfluidic devices.

Fabrication of optical elements by deposition of optical materials on glass or silicon wafer has been reported. However, this Micro Electro-Mechanical (MEM) technique requires special equipment and cleanroom facilities used in the semiconductor industry. A good alternative to the MEMS technique is soft lithography where optical elements can be created using polymers. In this work, ultraviolet-sensitive photo resists SU8 is used to fabricate the microfluidic cell sorting

devices and the optical elements. By using the mask with the patterns of the microchannel network and optical elements, the optical elements can be fabricated with the microchannel, eliminating the problem of alignment. Experiments are also conducted to evaluate the integrated optical elements.

To prevent cross-contamination, samples are usually prepared and are only mixed inside the microfluidic devices by the embedded mixers. Such embedded mixers, however, pose a great challenge as the small characteristic length of a microfluidic device tends to give a laminar flow and diffusion-dominated mixing. A simple passive micromixer is investigated to find the possibilities to integrate it to the microfluidic devices. To truly understand the diffusional mixing, a Y channel mixer is studied through the numerical and experimental investigations. Based on the results found, a possible design is also proposed and evaluated by experiments.

Acknowledgements

I would like to extend my greatest gratitude to my supervisor, Prof. Carolyn Ren, from whom I learned immensely during my studies. Her support and encouragement which helped me reach my educational goals are truly appreciated. I would also like to thank my co-supervisor Emily Moore, Santiago Faucher for their continual guidance throughout this work.

The knowledge and efforts of my colleagues in the Microfluidics and Biochip Research Group provided a resource that was valuable for successful completion of this project. In particular, Jay Taylor, Tom Glawdel, Razim Samy, Zhanjie Shao, Dr. Lin Gui, and Dr Junjie Ou are thanked for their contributions in creating a successful research facility.

I would like to thank Xerox and NESER for their financial support through a NESER Scholarship. Program is gratefully acknowledged.

My family support is throughout my studying. Without their support in my life, it is impossible for me to concentrate on my study.

Table of contents

List of Figures

List of Tables

Nomenclature

Acronyms:

LOC	Lab-on-a chip devices
PDMS	Polydimethysiloxane
CCD	Charged Coupled Device
CFD	Computational Fluid Dynamics
DI	De-Ionized
DPI	Dots per Inch
EDL	Electrical Double Layer
FACS	Fluorescence-Activated Cell Sorter
FWHM	Full-Width Half-Maximum
HV	High-Voltage
LED	Light Emitting Diode
MEMS	Micro Electro-Mechanical Systems
NA	Numerical Aperture
PCR	Polymerase Chain Reaction
PEB	Post Exposure Bake
PMT	Photo-Multiplier Tube
PDMS	Poly (dimethylsiloxane)
µAPD	Micro Avalanche Photo Diode
µFACS	Micro Fluorescence-Activated Cell Sorter
µPIV	Micro Particle Image Velocimetry
µTAS	Micro Total Analysis System

Mathematical Symbols:

C_i	Molar concentration of the *ith* species
d	Focused sample stream width
dp	Particle diameter
D	Diffusion coefficient of ions in EDL
Di	Diffusion coefficient of species *i*
e	Magnitude of a proton or electron charge (e = 1.602 x 10-19 C)
$\boldsymbol{E}$, $\vec{E}$	Electric field vector
Ex , Ey , Ez	Electric field strength in x-, y-, and z-directions
h, H	Channel height
k_b	Boltzmann constant (kb = 1.381 x 10-23 m2kg/s2K)
L	Channel length
n	Index of refraction
n_i	Bulk ionic concentration of the *ith* species
p	Pressure
Pe	Peclet number
Q	Volumetric flow rate
r_m	Radius of meniscus
$Rhyd$	Hydrodynamic resistance of microchannel
Re	Reynolds number
$Tabs$	Absolute temperature
$\boldsymbol{u}$, $\vec{u}$	Fluid velocity vector
u, u_{ave}	Average velocity
u_{eof}	Helmholtz-Smoluchowski velocity
u_{slip}	Slip velocity

Chapter 1 Introduction

1.1 Background

There has been an increasing trend towards the use of microfluidic devices usually called Lab-on-a chip devices (LOC) or micro-Total Analysis systems (μTAS) for bio and chemistry analysis in the last decade. This has resulted in:

- a **decrease** in reagent consumption and waste
- a **reduction** of cost per analysis
- **faster** analyses and results within a few seconds
- **safer** chemical experiments and reactions
- **improved** data quality
- **better** controllable process parameters in chemical reactions
- **increased** resolution of separations

By adopting the fabrication technologies of Micro Electro-Mechanical Systems (MEMS), it is possible to scale down bench top system in drug discovery, drug delivery, clinical diagnostics, genetics research, bio-weapons detection, and immunology(Fitzgerald 2002).

Most of the microfluidic devices are fabricated on microscope glass slides while silicon wafer is usually used for MEMS. A typical microfluidic device has to be integrated together with other components, such as pump, valves connecting with channel to conduct and control fluid transport, like a macroscopic system. Analogous to the bench top instruments, the corresponding detection system to identify species labelled by specific molecular in the fluid is also fabricated with the microfluidic device, making it possible to miniaturize the microfluidic device which is portable for on-site analysis in real time.

Even though MEMS technologies have been shown possible to be implemented in the fabrication of LOC device, there are many challenges yet to be tackled. For example, the cycle to fabricate a LOC device is usually very long, normally up to one week, making the cost high. Furthermore, clean-room facilities, which are often required for MEMS, are not suitable for the less-clean process of making LOC devices. Soft lithography (Xia and Whitesides 1998) offers a possible chance for microfluidic research at a relatively low cost and a very short fabrication cycle.

Construction of LOC devices using soft lithography relies on a specialized casting technique using polydimethysiloxane (PDMS). At first, masters called mode are fabricated by photolithography. PDMS is then poured onto the masters and a reverse pattern of the masters is created when the PDMS is peeled off from the masters. The PDMS with the intended pattern created earlier is then bonded onto a glass slide or a flat plate for the fabrication of the LOC devices. With soft lithography, only half to one day is sufficient to make LOC devices. The other advantage of soft lithography over traditional MEMS fabrication is low cost. PDMS and the equipment used are far cheaper than that needed for MEMS. Furthermore, there is no requirement of clean-room facilities.

Despite the advantages offered by the soft lithography technique, one great challenge with soft lithography is the precision alignment during the fabrication process. With the dimensions of the channel down to the order of micrometer, many phenomena, such as capillary force and gravity, become dominant and cannot be neglected as in the case in macroscopic. Even the weak electric potential (Zeta potential) formed at charged wall may be used to construct elecoosmostic pump (EOF pump) to drive fluid in microchannel. In most of cases, turbulent is unexpected and laminar flow is popular, so mixing in LOC devices is obviously slower since mixing is conducted by diffusion.

Despite above-mentioned challenges with LOC devices, there is a trend of ever increasing demand for miniaturizing bench top system in a single LOC device because of the excellent advantages of LOC devices over the bench top system. LOC devices hold the promises of ease of use and portability. For example bench top cytometry system is very complicated and can only be run in lab by professional operators. Scaling down bench top system like cytometry is feasible in theory; however there are many issues ahead.

Basically the most common pumps used to manipulate fluid or cells in microchannel are pressure-driven and EOF pumps with the latter being more popular and preferred. An EOF pump can be easily implemented by inserting an electrode in reservoirs. It has high response time; however a high power supply is required. In some applications, a pressure-driven pump has to be used when the flow does not support an EOF flow, such as organic solution or electric-sensitivity living cell in solution.

As mixing is quite often demanded for sample preparation and analysis, many research groups in microfluidic community get started in micromixing recently. Except for pumping, if extra energy input is introduced, the micromixing is active mixing; if not, it is passive. For passive micromixing, many complicated micromixers were reported and studied in Lab. On the market, there are passive micromixers made with metal (IMM). However, it is very hard to investigate the mixing process in metal micromixer since metal is not transparent.

Based on the optical detection method which has been widely used in chemistry or bio analysis, transferring the corresponding detection methods in LOC devices are developed simultaneously with microfluidic devices. As the amount of sample consumption with LOC devices decreases, the signal is also lowered. Nowadays, the continual advancement in technologies of micro-fabrication offers possible opportunities to have high sensitive optical sensor in microfluidic devices. Even though microfludics has been extensively studied in the last decade, there are a lot of challenges yet to be tackled.

1.2 Justification of Research

Integrated optical elements in the microfluidic cell sorting devices were designed and fabricated(Lee, Lin et al. 2003). But the truly portable LOC devices which operate without bulky optical instrument involved have not been reported. Due to the lack of the reliable and highly sensitive detection methods, the LOC devices which should be made portable and able to run even at home may not be used widely. The first part in this work deals with integrated optical coupler, waveguide and beam splitter for detection improvement.

Although PDMS has been widely used to fabricate LOC devices for the microfluidic research, the special LOC devices PDMS-SU8-silicon chip has to be fabricated with available material and equipment in lab due to the special requirement on the material refractive property of the optical components. Compared to the PDMS, SU8 gives a higher refractive index which is required to achieve total inter-reflection.

It has been long desired that a microfluidic device shall have a complete system which can perform one complete analysis. More complicated LOC devices with integrated multi-

components or units in one device have been developed. At the very beginning, micromixers were not considered in the field of microfluidics because laminar flow poses a great challenge that mixing in microfluidic device is done only by diffusion. Typically, small dimensions of LOC devices result in laminar flow. Without the eddy and convection of turbulence, micromixing is very slow and inefficient since only diffusion can contribute to mixing. This has resulted in more attention being channelled back to fabricate highly efficient mixing in a microfluidic device in the past few years. Either active micromixer or the passive micromixer comprised of very complicated channel network is used to promote mixing. However, simple passive micromixer is what microfluidic community are expecting. In the second part of this work, the micromixer is investigated broadly from simple Y channel design to the proposed inter-digital and porous mixer.

1.3 Objective of Thesis

This thesis is divided into two parts, with the first focuses on the investigation on the integrated optical elements in microfluidic cell sorting devices and the second on micromixer. The main goals of the thesis are described in the followings:

1. Apply microfluidic theory to design pressure-insensitive cell sorting device by implementing hydro-resistance component in the devices
2. Conduct an iterative design process to investigate and evaluate integrated optical elements for cell sorting device
3. Find the fundamental of micromixing through experiment and numerical simulation on simple Y channel micromixer
4. Design an inter-digital micromixer and a simpler porous micromixer
5. Investigate the performance of the proposed micromixer through experiment and numerical analysis

An overview of the fundamental microfluidic concepts and their applications in bio and chemistry analysis is first presented in Chapter 2. In the chapter, the advantages of microfluidics over conventional instrument are discussed. Subsequently, the corresponding theories and mathematic equations which describe hydrodynamic properties of fluid in microchannel are introduced. The optical detection for microfluidic cell sorting and the challenges for mixing performed on microfluidic device are also introduced and summarized in the chapter.

In chapter 3, the experimental setup for both topics is described detailed. The chemical materials, microscope and peripheral apparatus for pumping used in the experimental are discussed in detail.

Chapter 4 begins with the design for microfluidic cell sorting device. The issues involving in designing microfluidic cell sorting devices will be presented in detail. These include hydrodynamic focusing for accurate detection, undesired pressure-induced flow. A shallow channel to reduce pressure-induced flow, and its actual implementation on microfluidic cell sorting devices, are described in detail.

The integrated optical elements are summarized and addressed in chapter 5. Experimental setup for integrated optical detection is introduced. Such setup includes external instrument, laser, optical sensor PMT, HS488 programmable power sequencer for implementing EOF flow, and data processing and system control application software programmed with LabView. Different designs are tested with the experimental setup. The final results are presented and discussed.

In chapter 6, different micromixers are investigated to find the possibilities to fabricate a simple and easy-use micromixer. Based on a simple Y channel, experiments were carried out to investigate the mixing on microfluidic devices and get the dominant factors that influence the mixing efficiency. In the second half of the chapter, two simple mixers are proposed. They are: interdigital mixer and porous micromixer. For the interdigital mixer, numerical analysis is set in COMSOL. In the analysis, the model is significantly simplified due to the expensive cost on available computer source. Finally, the experimental verification is conducted and results are discussed.

The last chapter summarizes the work done and the findings on the two key topics. Recommendations for future works developments are also outlined.

Chapter 2 Literature Review

2.1 Background

Developing a Lab-on-a-chip device requires the input from different disciplinary, e.g. biology, chemistry mechanical engineering, physics and electrical engineering. While mechanical engineers focus on manipulating fluid and designing components which work along with LOC devices, biology and chemistry researchers verify the theory and design by using the state-of-the-art technology provided by mechanical engineers and feedback the specific requirements. Physics and electrical engineering also play a vital role in understanding the phenomenon and the fundamentals in the microscopic point of view. In other words it is impossible to develop a truly microfluidic device without any one of them. Mechanical engineer may model microfluidic devices through numerical analysis which will significantly reduce cost and time. Through designing and optimizing various components, such as pump, valve and mixer, mechanical engineers pave a straightforward road for biology and chemistry application.

This chapter addresses the fundamentals needed to understand microfluidics and it also extensively reviews the currently state of development in the optical detection integrated with microfluidic devices and micromixer. Common applicable theories which define microfluidic transport phenomenon, pressure, electrokinetic, mass and momentum transport are outlined in the first part of the chapter. The second part of the chapter introduces the design process using COMSOL numerical simulation. Brief fabrication technology and relevant issues are then described. This is followed by the current state in optical detection with LOC devices and micromixer.

2.2 Microfluidics for Biomedical Applications

The advantages offered by microfluidic devices over traditional instrument for chemical and biological analysis are the reason why microfluidics is considered one of many high technologies which will revolutionize our life in the near future.

Many of the systems used for analyzing biological samples are large bench top systems that incorporate a variety of sensors, laser light sources, complex fluid handling equipment, environment control systems and bio-analysis tools. The cost of such equipment is usually high and the duration of performing multiple tests is relatively long. By reducing the size of the fluid networks to the micro-scale, where one or more dimensions is 1 μm to 100 μm, the length of the channel becomes comparable to the size of the materials to be analyzed. This provides potentials for improved sensitivity of the system, drastic reduction in the time scales of diffusion and reaction and high throughput by means of parallelization (Stone, Stroock et al. 2004; Huh, Gu et al. 2005; Dittrich and Manz 2006).

The advantages of microfluidics have inevitably led to the replacement of large chemical synthesis and bio-analysis systems with lab-on-a-chip or micro total analysis systems. The size reduction of the overall system permits handheld, portable operation. The volume of sample or reagents required for operation is also decreased significantly. In circumstances where access to the sample is limited, forensic studies for example, volumetric savings may be critical. Cost and ease of manufacturing is improved by using microlithographic processes made popular in the microelectronics industry. Microscale systems also differ from macroscale and have a dramatically increased surface to volume ratio (Ho and Tai 1998). This condition enables unprecedented levels of control of heat and mass transfer. Alternative methods of driving flow become viable in microfluidics and one popular technique is electroosmotic flow.

The development of lab-on-a-chip devices is currently in a transition from concept to application. However, people are also still working at the design level trying to improve the functionalities of many of the primary components. The microfluidic chip can achieve higher performance efficiencies and consume less operating power, whether it uses applied potentials or pressure sources. Issues of device contamination, flow anomalies, blockages, and altered surface properties are relevant and need to be investigated further. Despite the difficulties encountered in the industry's infancy, several lab-on-achip systems have been developed and are sold commercially. The GeneXpert, a DNA extraction and polymerase chain reaction (PCR) amplification system has been developed by California-based Cepheid extracts DNA and RNA from blood samples or microbial spores for amplification and analysis. The reduced processing time for this device is 96-fold that of conventional systems (Clayton 2005). Other examples

include the BioMEMS-768 developed by GenoMEMS, the bench top Experion assay system from BioRad Laboratories, Agilent Technologies' 2100 BioAnalyzer, and Caliper Life Sciences' LabChip 90 devices which are capable of performing electrophoretic separation of protein, DNA, or RNA. The CytoChip, by CelTor Biosystems, is a drug analysis platform that simulates a precise biological environment. Invitrogen developed the PathAlert system which allows detection of infectious agents using PCR and analysis techniques. This device can be used to detect plague, anthrax, small pox, or tularemia pathogens. Benefits from the application of microfluidics are also expected in pharmaceutical research, drug delivery systems, and biological engineering research in addition to the diagnostic and analysis devices described above (Fitzgerald 2002; Clayton 2005). Several reviews have been published that outline the major developments and applications for lab-on-a-chip technologies: (Reyes, Iossifidis et al. 2002; Erickson and Li 2004; Vilkner, Janasek et al. 2004).

Fabrication of microfluidic chips employing lithography techniques was established in microelectronics manufacturing (Elliot 1986). The standard photo-lithography method provides high resolution channel networks etched in silicon or glass which can be directly bonded to another silicon or glass layer to form an enclosed chip. Photo-lithography can also produce positive relief structures that function as a mould for soft polymer replication. Both types of micromachining are performed by exposing a thin layer of photo-sensitive material, called photoresist, on the silicon or glass substrate through a patterned photomask and subsequently developing the soluble portions of the photoresist coating. The remaining photoresist acts as a mask during the etching process. As a quicker and more cost effective alternative, the recently developed soft-lithography method allows the creation of a similar positive relief mould without the stringent clean room conditions (Xia and Whitesides 1998), (McDonald, Duffy et al. 2000). The primary difference is that no etching is required due to the use of the patterned photoresist as the relief structures. In the casting process, a liquid elastomer mixture is poured on the chip mould and cured to solidify the replica. The solid replica containing the channel features is then reversibly or irreversibly bonded to a substrate of glass, silicon, or a similar elastomer.

Polymer (dimethylsiloxane) (PDMS) is a common replicating material due to its transparent optical properties, bio-compatibility, ability to transfer sub-micron features, gas permeability, and elastomeric mechanical properties that provide flexible, watertight interconnects (Li 2006)

(Rolland, Hagberg et al. 2004) (Quake and Scherer 2000). The main disadvantages of using PDMS, compared to glass or silicone, are the instability of surface properties over time, hydrophobic surface characteristics in its untreated state, and typically lower fluid mobility values.

2.3 Microfluidic Transport Phenomenon

As the length scale down to the order of micrometer, many physics negligible in macroscopic have to be considered under microfluidics. Surface forces, such as capillary and eletectrostatic forces, scale to the first or second order of the characteristic length while body forces, gravity and magnetic forces, scale to the third power (Ho and Tai 1998). Jean Berthier (Jean Berthier 2006) and Squires and Quake (Squires and Quake 2005) gave a detailed description of microscale physics and the following is a brief introduction.

2.3.1 Electrical Double Layer (EDL)

When in contact with an aqueous solution, most solid surfaces carry eletectrostatic charges or an electrical surface potential. There are an equal number of positively and negatively charged ions in solution which flow along microchannel. This means that the distribution of ions along cross section is not uniform from the microscopic angle as the solid wall carrying charges attract counter-ions, so the concentration of ions in solution is not uniform. Near the solid wall, counter-ions are attracted on the solid wall called compact layer or stern layer which is immobile. From compact layer to the bulk of the solution is termed as the diffusion layer. Compact layer and diffusion layer are together called Electrical double layer (EDL). EDL is very important to implement EOF flow in microfluidic device as illustrated by Hunter (Hunter 1981) and Li (Li 2004). Referring to the Figure 2-1, the potential called Zeta potential is between the two layers.

An estimate of the characteristic length of the EDL is determined by the expression for the Debye-Huckel parameter λ_D :

$$\lambda_D = \sqrt{\frac{\varepsilon_r \varepsilon_0 k_b T}{e^2 \Sigma z_i^{\,2} n_{i\infty}}} \qquad \textbf{2-1}$$

where ε_r is the dielectric constant of the solution and the permittivity of a vacuum $\varepsilon_0 = 8.854 \times 10 - 12C/Vm$, $k_b = 1.381x10^{-23} m^2 kg/s^2 K$ is Boltzmann's constant, $e = 1.602x10^{-19} C$ is the charge of an electron,, T is the temperature *(K)*, z is the ion valence and $n_{i\infty}$ is the bulk ion density. For a sample 100 mM buffer solution (valence = 1:1) in contact with glass, the order of the EDL is approximately 10 nm. The Debye length increases as the concentration of the electrolyte is reduced; water has a characteristic EDL thickness of 300 nm. The EDL thickness for most buffer solutions in microchannels greater than 10 μm can be considered negligible.

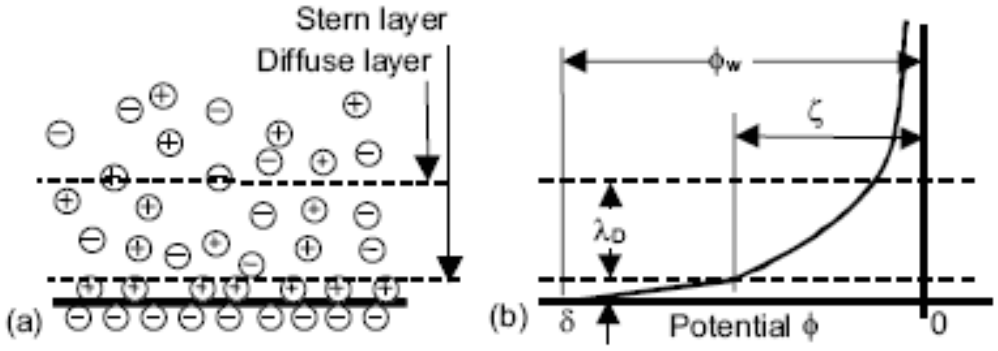

Figure 2-1 Schematic of phenomena occurring in the electric double layer (EDL): a) the stern layer and diffusion layer and b) the resulting potential (Nguyen 2006).

The Zeta potential depends on many factors, such as fluid-solid interaction, pH value of the fluid and temperature. In this work, a glass-PDMS chip is fabricated and a 50mM sodium (bi-) carbonate buffer solution in the chip generates a negative charge in the order of -80mv.

2.3.2 Fluid Flow

Compared to the mean free path of the liquid molecules (0.3nm), continuum hypothesis is still holding because the length scale is large enough. The Reynolds number, Re, is less than 1 due to the small length scale, so viscous effect is equal or more significant than inertia effect and Stokes'

equation is used to analyze and assist design process instead of N-S equation. Although surface forces including capillary and electrostatic forces for microfluidic devices extremely affect fluid flow, it can be neglected in the macroscopic. Therefore, many unknown aspects have to be investigated to truly understand microfluidics.

While the length scale decreases down to the order of micron, many mechanisms of transport phenomena including momentum, energy, and mass transport have to be modified. The principles and theories of fluid mechanics well-built previously in macroscopic area are still applicable to microfluidics. The followings only serve as a brief introduction of the basic concept and equations. More detailed work on the fluid mechanics and transport phenomena have been covered in the texts by White (White 1999) and Bird (Bird 1960) respectively. The fundamentals and electrokinetic flow of microfluidics can also be found many of th recently published texts (Hunter 1981), (Masliyah 1994), (Li 2004), (Tabeling 2005), (Nguyen 2006).

As the length scales down to the order of micrometer, many micro-phenomena, such as Laplace pressure from meniscus and charged wall between channel and fluid flow, have to be re-evaluated. Due to the fact that the charged wall attracts counter-ion in flow to the wall and modifies distribution of ions in liquid flow along cross section, the local concentration of counter-ions close to the wall is higher than that in the middle of the channel, leading to the formation of an electrical potential called Zeta potential (Hunter 1981).

Normally, the N-S equations are applicable in the area of microfluidics when

$$Kn = \lambda / L < 1$$

where

- λ = mean free path (m)
- L = representative physical length scale (m)
- *Kn :Knudsen Number*

The characteristic length is over 1um for microfluidic devices and some can be 10 or up to 100 um. Since liquid flow in microchannel results in a 0.3um mean free path length of liquid molecules, the N-S equations are still working in microfluidics. General form of N-S equation is as follows:

$$\rho[\frac{\partial \vec{u}}{\partial t} + (\vec{u} \cdot \vec{\nabla})\vec{u}] = -\nabla \vec{p} + \mu \vec{\nabla}^2 \vec{u} + \vec{F} \quad \textbf{2-2}$$

The right-hand-side represents inertia effect which is a nonlinearity term. $\vec{F}$ represents "other" body forces (forces per unit volume), such as gravity or centrifugal force, p is the pressure, μ is the solution viscosity, and ρ is the solution density.

As length scale down to micrometer, the gravity becomes negligible. The electrostatic and surface forces have to be involved instead. And the right-hand-side shrinks down to zero which gives us Stokes' equation as the following:

$$\nabla \vec{p} = \mu \vec{\nabla}^2 \vec{u} + \vec{F} \quad \textbf{2-3}$$

Since the liquid flow in microchannel is imcompressible, so the continuum equation together with stokes' equation become the governing equation group to be used to numerically analyze and design LOC devices.

$$\vec{\nabla} \cdot u = 0 \quad \textbf{2-4}$$

2.3.2.1 Electroosmotic Flow (EOF)

When the polarity solution contacts with the wall of channel typically charged with electrons, Zeta potential is naturally generated. As applying electric field at ends of the channel, the built-up counter-ions close to the wall will be moved by applied electric field. The counter-ions further drag the bulk of fluid away from wall to move due to viscosity effect. Under the steady state, the Stokes' equation is further simplified to become:

$$\nabla \vec{p} = \mu \vec{\nabla}^2 \vec{u} + \vec{F} \qquad \textbf{2-5}$$

Therefore, without considering other body forces and pressure-induced flow, The Stokes' equation above is re-written:

$$0 = -\nabla \vec{p} + \mu \vec{\nabla}^2 \vec{u} + \rho_e \vec{E} \qquad \textbf{2-6}$$

Where ρ_e is the net charge density and $\vec{E}$ is the electric field vector defined by the potential field:

$$\vec{\nabla} \cdot (\sigma \vec{\nabla} \phi) = 0$$

$$E_x = -\frac{\partial \phi}{\partial x},\ E_x = -\frac{\partial \phi}{\partial x},\ E_x = -\frac{\partial \phi}{\partial x} \qquad \text{2-7}$$

where σ is the fluid electrical conductivity, ϕ is the applied potential field, and E_x , E_y and E_z are the electric field strength in the x, y, and z directions, respectively.

From the Poisson equation, the electrical potential generated by the surface charge can be presented as the following:

$$\vec{\nabla}^2 \psi = -\frac{\rho_e}{\varepsilon} \qquad \textbf{2-8}$$

where ψ is the electrostatic potential and ε is the fluid permittivity. The ionic concentration of the i^{th} species in the EDL may be modelled by the Boltzmann distribution:

$$n_i = n_{i\infty}\, exp(-\frac{z_i e \psi}{k_b T}) \qquad \textbf{2-9}$$

Hence the net charge density is given as the following:

$$\rho_e = e \sum_i z_i n_{i\infty} \exp(-\frac{z_i e \psi}{k_b T}) \quad \textbf{2-10}$$

Considering a very simple case, the flow in the x-direction is generated between two plates, separated in the z-direction (Tabeling 2005), the following ca be derived:

$$0 = -\frac{\partial p}{\partial x} + \mu \frac{\partial^2 u}{\partial z^2} - \varepsilon E_x \frac{d^2 \psi}{dz^2} \quad \textbf{2-11}$$

In the absence of a pressure gradient (assuming the same hydrostatic head at ends of channel and capillary forces), both potential and velocity gradient are set to zero at the edge of the EDL. At the wall, the potential is Zeta potential and velocity is zero. Thus, the following equation is resulted by integration (Tabeling 2005):

$$u(z) = \frac{\varepsilon E_x}{\mu}(\psi - \zeta) \quad \textbf{2-12}$$

where ζ is the zeta potential. Looking back to the Figure 2-1, the potential is going down to zero outside the EDL, so the velocity distribution along z-direction becomes:

$$u(z) = -\frac{\varepsilon \zeta}{\mu} E_x \quad \textbf{2-13}$$

Normally $u(z)$ is rewritten as u_{eof} called the Helmholtz-Smoluckowski velocity. $-\frac{\varepsilon \zeta}{\mu}$ is rewritten as μ_{eof} called the electroosmotic mobility. From 2-15, the linear relationship between velocity and electric field can be derived. So the plug-like velocity distribution along the cross section of the channel could be acquired under the EOF flow.

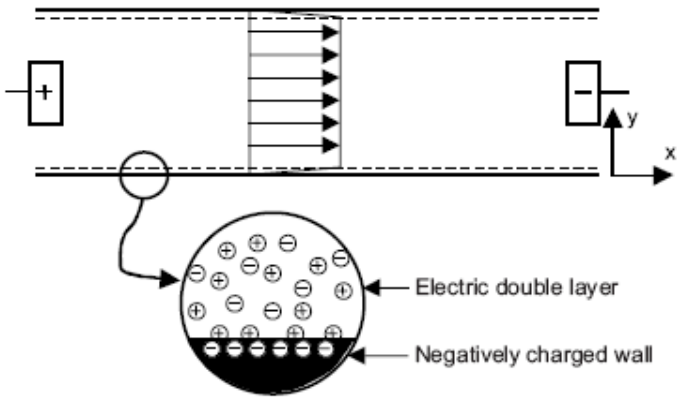

Figure 2-2 Schematic representation of the flow in a constant cross-section channel subject to electro-osmosis. Extra counter-ions at the charged surface are driven by the applied electric field and drag the surrounding bulk fluid by viscous forces. A plug-like velocity profile is achieved(Nguyen 2006).

The plug-like velocity of EOF flow offers us many advantages over parabolic velocity by pressure-driven flow. Firstly, the plug-like velocity minimizes sample dispersion and reduces the velocity variation. Secondly, it is easier to implement EOF flow through inserting electrodes into reservoirs or pattern electrodes on substrate which introduce electrical field in microfluidic device. Pressure-driven flow requires the special connector to bridge pressure pump with microfluidic device. Thirdly EOF pump has fast response time. This means that EOF has a better control over the flow rate or to switch flow by simply changing electric power supply.

Though EOF offers numerous advantages, it is, in fact, it is very hard to achieve pure EOF flow. The different liquid level at each reservoir of the microfluidic device is often resulted when the liquid is transported from one reservoir to the other. Furthermore, electrodes used also induce extra surface forces. Although the big reservoirs may reduce the curvature radii of interface, it is impossible to completely remove surface force by meniscus. The other possible factors affecting velocity distribution in the channel include fluid evaporation that leads to the different level in each reservoir and the bubbles generated around electrodes due to the electrolysis that also cause mobility change in the channel.

2.3.2.2 Pressure-Driven Flow

Pressure is widely employed to drive fluid in a channel. In the area of microfluidics, the flow should be laminar in most of cases and flow rate can be presented by the Hgen-Poiseuille law:

$$Q = \frac{\Delta p}{R_{hyd}} \qquad \textbf{2-14}$$

where Q is the flow rate, p is the pressure and R_{hyd} is the hydrodynamic resistance. (Beebe, Mensing et al. 2002) gives the following equation:

$$Q = \frac{\Delta p w h^3}{12 \mu L}\left\{1 - \frac{h}{w}\left[\frac{192}{\pi^5}\sum_{n=1,3,5}^{\infty}\frac{1}{n^5}\tanh\left(\frac{n\pi w}{2h}\right)\right]\right\} \qquad \textbf{2-15}$$

For the flow in high aspect ratio $h>>w$, it can be rewritten into

$$Q = \frac{\Delta p w h^3}{12 \mu L} \qquad \textbf{2-16}$$

Comparing 2-16 with 2-18 so we have:

$$R_{hyd} = \frac{12 \mu L}{w h^3} \qquad \textbf{2-17}$$

From 2-19, the same flow rate can be achieved through increasing Hydroresistance if higher pressure gradient is present along the channel.

2.3.2.3 EOF-Pressure Hybrid Flow

Even though EOF flow is preferable, the hybrid flow could be experiencing due to the hydrostatic head, different meniscus in each reservoir. To achieve pure EOF flow in microfluidic devices, the

best way is to decrease pressure driven flow through implementing hydro-resistance components during the design process.

Meniscus is called Laplace pressure and actually a kind of surface force. Surface force is definitely generated at the interface when the fluid (gas or liquid) is brought to contact to solid or other fluid due to different surface energy. Referring to the Figure 2-3, let us talk a little bit about surface forces.

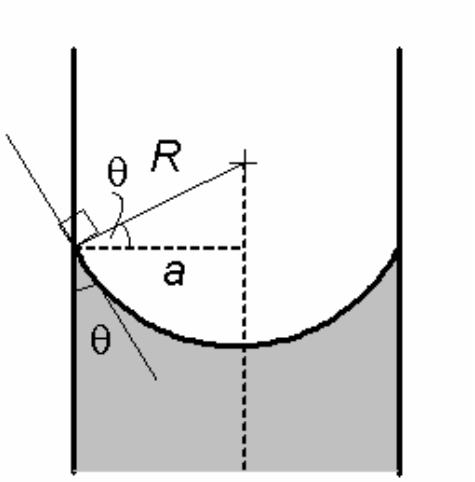

Figure 2-3 Spherical meniscus with wetting angle less than 90°

Commonly, Young–Laplace equation is used to model this physics:

$$\Delta p = \gamma(\frac{1}{R_1} + \frac{1}{R_2}) \qquad \textbf{2-18}$$

where:

- Δp is the pressure difference.
- γ is surface tension.
- R_1 and R_2 are radii of curvature in each of the axes that are parallel to the surface.

The pressure is also called Laplace pressure. The quantity in parentheses on the right hand side is in fact just or twice the mean curvature of the surface depending on normalization. With this the equation is simplified into the following:

$$\Delta p = \frac{2\gamma}{R} \qquad \textbf{2-19}$$

(Walker and Beebe 2002) employed Laplace pressure to induce pumping in a microchannel. The magnitude of the pressure generated for water ($\gamma = 72.8mN/m$) forming a hemispherical meniscus in a reservoir with a radius of 1mm is 146 Pa. The resulting flow of water through a 50 mm long channel of square cross-section with 50 μm sides produces a linear flow rate $\vec{u}_{laplace} = 257\,\mu m/s$. It is almost the same magnitude as most microfluidic applications.

2.3.3 Mass Transport

The mass transport is a common phenomenon in bio or chemistry analysis in microfluidic device. Hence understanding mass transport is crucial in order to understand operation of mixing or sample preparation. The single specie in a flow field is governed by the advection-diffusion equations(Masliyah 1994):

$$\frac{\partial c_i}{\partial t} + \vec{u}\cdot(\nabla \vec{c}_i) = D_i(\nabla^2 \vec{c}_i) - \frac{D_i z_i e}{k_b T}\nabla\cdot(\vec{c}_i \vec{E}) + R_i \qquad \textbf{2-20}$$

where c_i is the molar concentration of species *i,* D_i is the diffusion coefficient of species *i*, z_i is the valance of the species, e is the electron charge, $\vec{E}$ is the applied electric field and *Ri* is the rate of generation of species *i*. For the laminar flow, the convection term should be cancelled out, so the equation shrinks down to Fick's law. Mixing in microfluidic devices is thus diffusion-dominant which leads to very slow mixing.

2.4 Numerical Analysis for Microfluidic Design

Numerical or analytical solution to evaluate new design aids to significantly shorten the design process and reduce the cost. The corresponding mathematic descriptions for the phenomenon experienced in microfluidic devices have been discussed earlier. Under the reasonable and appropriate assumptions and taking the right boundary conditions, the mathematic description could be simplified to get some analytical solution. Even if the model could not be simplified, the numerical analysis may also be useful to guide design. (Erickson 2005) offered a review on the various numerical techniques to solve the microfluidic problems from fluid flow, mixing, electroosmotic flows, magnetic phenomenon, and acoustics and so on.

Analytical solutions are readily available for the simple network channel. For the complicated design, numerical simulation has to be set up to get rough idea about new design. On the market, many available commercialized softwares such as ANSYS, Conventer, CFDACE and COMSOL Multiphysics can be used in microfluidic numerical simulation. Moreover, there are some written in house software with general programming language such as Fortran, C/C++ and Matlab (Erickson 2005). Among them COMSOL Multiphysics is employed most of time because of its easy-use and many built-in modes on microfluidics.

In COMSOL, the geometry mode should be set up at first. Geometry is first drawn and then impoted using built-in drawing tools or other AUTOCAD tools. The mesh is generated by clicking the corresponding tool. The mesh size can be adjusted through setting the parameters. Numerical simulation can be conducted once the boundary conditions and coupling variables are set.

Comparing the channel network of the microfluidic devices with circuit, there are many similarities between them so several researchers have developed simplified compact circuit model. (Fletcher, Haswell et al. 2001) developed a circuit based model to solve electrooamotic flow in a microfluidic network using the resistance based elements. The similar models are also addressed by (Qiao and Aluru 2002) and (Chien and Bousse 2002).

2.5 Fabrication of Microfluidic Devices

The microfluidic devices originated from MEMS which are commonly fabricated in silicon, glass or quarts using photography technique. Due to the long cycle of the MEMS fabrication, expensive equipment and cleanroom are often required. However, with the introduction of soft lithography and availabilities of polymer materials, microfluidics design based on MEMs techniques has been extensively studied.

2.5.1 Soft lithography

Soft lithography is similar to the photography technique well-established with MEMS. It refers to a specialized subset of casting techniques which uses PDMS and a rapid prototyping framework to fabricate microfluidic devices. Originally developed by (Xia and Whitesides 1998), soft lithography consists of two steps. At first the master called molding is fabricated on glass or silicon wafer and then pouring PDMS (dimethysiloxane) on master to replicate it so that reverse pattern is transferred into PDMS. To transfer pattern on the wafer coating with photoresists SU8, the mask designed with AUTOCAD tools and printed out using high resolution printer is used. The patterned PDMS is brought to substrate to build PDMS chip.

2.5.2 PDMS-Glass Chip

PDMS-Glass (PG) chip are widely used in the field of microfluidics because they are much cheaper than whole glass chip. Bonding of PDMS onto glass is also simpler than onto a glass chip. Normally the latter requires high pressure and temperature.

To make PDMS-Glass chip, the pre-cured liquid PDMS is mixed with cured agent and then poured over the master, and cured in over at 80 degree. After one hour or slightly longer, the solidified PDMS is peeled off from master. temporary bonding can be achieved simply by placing the PDMS on glass or silicon substrate, or using plasma to treat both substrate and PDMS prior to placing them together (McDonald, Duffy et al. 2000).

2.5.3 PDMS-SU8-Silicon/Glass Hybrid Chip

Although PG chips have been widely used and almost become the standard in microfluidic research, some special chips are preferred by some researchers. Due to the fact that the PDMS is absorbent to small molecules and flexible, PG chip will lose its advantages when small molecule chemical is used.

PDMS-SU8-Silicond/Glass chip is shown as Figure 2-4. For this kind chip, the microchannel is directly patterned on the wafer coating with SU8. After developing, the unexposed area is removed by development chemicals. With flat PDMS to cover the top of the channel, the PDMS-SU8-Silicon/Glass hybrid chip could be fabricated. However the cost is higher than the PDMS chips. As SU8 gives higher refractive index over 1.45 (Lin, Chang et al. 2002; Ruano-Lopez, Aguirregabiria et al. 2006), it is easy to implement optical components in SU8 Layer.

Figure 2-4 Illustration of PDMS-SU8-Silicon/Glass chip

2.6 Integrated Optical Waveguide for Cell Sorting

In this work, the integrated optical elements are implemented on the microfluidic device to improve detection sensitivity so that it makes possible a truly portable microfluidic device. So the counterpart bench-top system is discussed briefly to give us a concept and then detail discussions are focused on the optical detection which is needed to be adapted into the mircrofluidic devices.

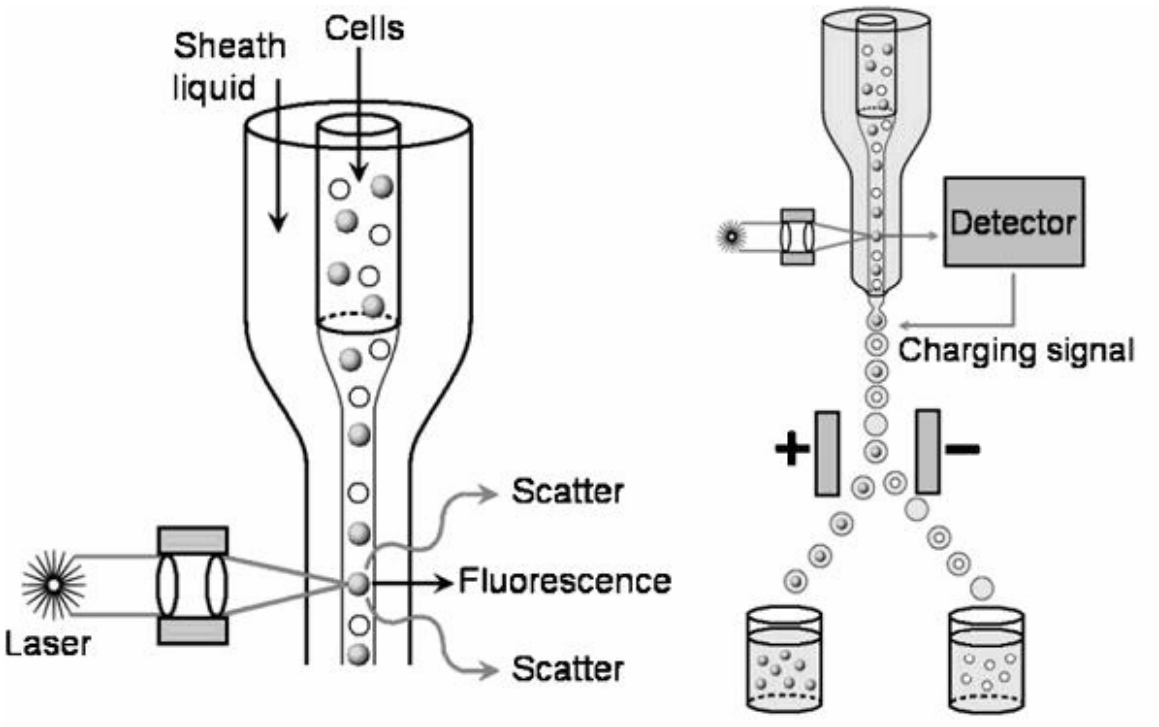

Figure 2-5 Schematic of a conventional FACS droplet sorter. Detection is performed on individual cells in a focused stream. Formed at the nozzle, droplets containing target cells are charged upon exiting the nozzle and deflected by charged plates into a collector(Huh, Gu et al. 2005).

A typical instrument for cell sorting is shown as Figure 2-5. (Recktenwald 1998),(Shapiro 2003) and (Melamed 1990). These systems incorporate a series of laser light sources and light sensing units that capture information about the cells transported through the detection region as a suspension in a liquid stream. This system employs a sheath fluid that hydrodynamically focuses the cell suspension. The particles contained within the sample fluid pass through a specific location where the cells can be uniformly illuminated by focused laser beams. Derived from the light scattering and fluorescent emissions, some cell cytometers can detect up to 12 fluorescent colours and have the capability to determine the size of particles, granularity of the cytoplasm, cell shape, membrane potential, intracellular pH, and cell viability. Cell cytometers can also quantify the intracellular levels of DNA, RNA, proteins, lipids, antigens, enzyme activity, and surface receptors (Rieseberg, Kasper et al. 2001). This analysis can be performed at frequencies up to 25 kHz. From the bench-top system, three main functions are identified: sample focusing, detection and sorting.

This bench-top instrument is very expensive and run by specialist in lab. To achieve on site and real time diagnosis which is highly demanded by the bio-medical analysis, the environmental and food monitoring, miniaturizing it is highly demanded and Microfluidics could be the solution of this issue.

(Taylor 2007) described mcirofluidic devices for cell sorting and counting and evaluated it through numerical analysis and experiment. However the bulk light source from microscope has not been removed. A similar device was also reported by (Yang, Hsiung et al. 2006) with the external optical detection approach.

Basically the configuration of the external optical detection for the microfluidic devices generates very weak signal due to the tiny amount of the sample going through the detection point. Naturally embedded fibre and integrated waveguide to guide excitation sources close to the sample flow are used because of the very low power loss of the excitation sources. A devices with two embedded fibres for two-point detection was reported by (Xiang, Xuan et al. 2005) so that the velocity of the particles or cells could be derived. The fibre put on some limits on the reported devices. The whole chip has the same height as the fibre diameter. Many challenges should be suffered by inserting fibre in the chip. (Lin and Lee 2003) reported one device with one embedded fibre.

Integrated optical waveguide to guide light source to detection point can exceed the method using embedded fibres because it removes the limit from the fibre and reduces the possibilities of breaking the fibre during inserting fibres. (Ruano-Lopez, Aguirregabiria et al. 2006) reported a device with one integrated SU8 waveguide and characterize the SU8 waveguide. This waveguide is straight one so little of power loss was experienced. The similar devices are also reported by (Lee, Lin et al. 2003).

An interesting device with integrated optical elements including beamsplitter, waveguide and coupler was reported by (Ruano, Glidle et al. 2003). In that paper, the detail description about beamspliter and bending waveguides were presented. Using Flame Hydrolysis Deposition of glasses, the silica optical elements are fabricated on silicon.

Some interesting works have also been carried out to further miniaturize microfluidic cell sorting devices. For example (Kuo, Kuyper et al. 2004) and (Miyaki, Guo et al. 2005) incorporated high-power light-emitting diodes(LEDs) as light sources. Chip-mounted photodiodes have been used to replace photo-multiplier tubes (PMT) to pick up signal (Kamei, Paegel et al. 2003),(Jorgensen, Mogensen et al. 2003) and (Chabinyc, Chiu et al. 2001).

2.7 Micromixers

Mixing is a physical process with the goal of achieving a uniform distribution of different components in a mixture, usually within a short period of time(WolfgangEhrfeld 2000). Among the mechanisms known for mixing of liquid phases, molecular diffusion is the final step in all mixing processed. Diffusional transport obeys Fick's law which correlates to the change of concentration with time and hence to the product of the diffusion coefficient and concentration gradient. By rearrangement of this relationship, the following equation results:

$$t \sim d^2 / D \qquad \textbf{2-21}$$

Where t is the mixing time, d is the width of channel, D is the diffusion coefficient. Mixing therefore depends on the diffusional path d. In a turbulent regime the fluid entity constantly is subdivided into thinner and thinner by an induced circular motion of fluid compartments, so-called eddies, and subsequent breaking into fragments (see **Figure 2-6**).

Figure 2-6 Schematic of the creation of eddies by stirring (turbulent mixing)(WolfgangEhrfeld 2000).

In a laminar regime, a similar breaking of fluid compartments cannot occur due to the high viscous forces. Instead, the fluid entity has to be continuously split and recombined; forming regularly-sized fluid embodiments (see Figure 2-7). As a vivid example, this process is similar to the cutting of slices from two different solid blocks, and subsequent alternate stacking of the slices to give a joint assembly. Multiple repetition of this procedure finally leads to a dispersed solid body.

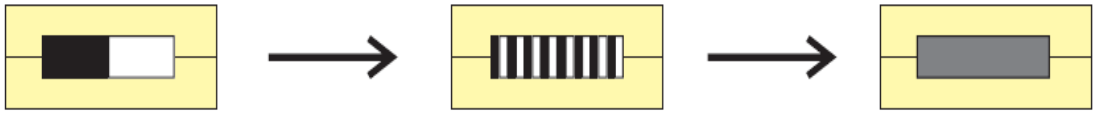

Figure 2-7 Schematic of the splitting by continuous geometric separation and reunion of fluid embodiments (laminar mixing)(WolfgangEhrfeld 2000).

Most of mixing in microfluidic devices is diffusional mixing due to the laminar flow. To achieve a fast mixing, many methods have been employed either to reduce diffusional path or induce chaotic flow using complicated 3-D design.

Micromixers are categorized as the active and passive mixing (Nguyen and Wu 2005). Passive micromixers do not require external energy, so the mixing process relies entirely on diffusion or chaotic advection. Active micromixers use the disturbance generated by an external field for the mixing process. Furthermore, external power sources are needed for the operation of active micromixers. Thus, the integration of active mixers in a microfluidic system is both challenging and expensive. In contrast, passive micromixers do not require external actuators except those for fluid delivery. The often simple passive structures are robust, stable in operation and easily integrated in a more complex system.

Based on Y or T microfluidic devices, mixing at extremely high Reynolds numbers could also result in a short mixing length(Yi and Bau 2003; Wong, Ward et al. 2004). A very high pressure which generates high velocity and Re number can be a big challenge for bonding and interconnection technologies. The basic T-design can be improved by roughening the channel wall(Wong, Bryant et al. 2003) or throttling the channel entrance (Gobby, Angeli et al. 2001). At

high Reynolds numbers the basic T-mixer can be furthermodifiedwith obstacles, which generate vortices and chaotic advection.

Reducing the mixing path is the simplest method to improve mixing. A lamination mixer with 32 streams was reported to be able to achieve full mixing in 15 ms(Bessoth, deMello et al. 1999). This mixer type was successfully used in a practical analysis(Kakuta, Jayawickrama et al. 2003). The flow in micromixers based on parallel lamination is usually driven by pressure, but can also be generated by electro-osmosis as reported by (Fluri, Fitzpatrick et al. 1996; Hadd, Raymond et al. 1997; Jacobson, McKnight et al. 1999). Another concept of reducing mixing path for parallel lamination micromixers is hydrodynamic focusing (Knight, Vishwanath et al. 1998).

For the active micromixer, the extra energy such as electrical field for EOF flow or magnetic field to drive the magnetic beads can be used to induce the flow perpendicular to the mixing flow to enhance mixing. More detail about active micromixer will not be summarized furthermore. My focus is on the passive micromixers.

How to quantify the extent of mixing is important for evaluation of performance as well as design optimization of micromixers. The common quantification technique is using dilution of a tracer dye to determine the extent of mixing. The intensity image can be recorded and evaluated. Since the concentration of the dye is proportional to the intensity of the recorded image, the uniformity of the concentration image can be quantified by determining the standard deviation of the pixel intensity values(Liu, Stremler et al. 2000). The approach of recording images is statistical methods, which depend on the orientation of the mixed fluids relative to the imaging direction. If the imaging direction is perpendicular to the fluid layers as in the case of the mixer reported by (Hinsmann, Frank et al. 2001), the two layers, even at the channel entrance, appear to be completely mixed. In such cases, an imaging system with a con-focal microscope is required for the three-dimensional spatial distribution of the concentration field.

Another quantification method is tracing product of a chemical reaction. The products' color or pH value can be related to the mixing efficiency.

2.8 Summary

In this chapter, the background and fundamental on microfluidics are introduced. The mathematic descriptions of a broad range of transport phenomena in the microfluidic devices, as well as the fabrication process, are also discussed. Finally a review of micromixers and the integrated optical elements for cell sorting detection is provided. However, the community of microfluidics is still searching for a reliable integrated optical detection. For the micromixing, simple micromixer with high efficiency is still absent.

Several studies have reported integrated optical elements in the microfluidic devices which are able to improve the detection. Some of them are fabricated directly on SU8 layers or by filling SU8 into channel; however they are strait waveguide. But the optical elements such as beamsplitter and bending waveguide fabricated with SU8 have not been thoroughly investigated. The strait waveguide is simpler than bending one or beamsplitter. But the latter are essential to integrated optical elements in the mirofluidic devices.

In the past few years, the importance of the micromixers has been recognized, especially for the passive micromixers. To realize rapid mixing, the very complicated designs are often used to induce chaotic advection mixing; and the interdigital micromixers have already been emerged on the market. But soft lithography generates planar features so the fabricating 3-D mixers like the interdigital micromixer are very difficult.

Chapter 3 Experimental Setup and Procedure

The experimental system in this work involves optical, electrical and mechanical components, of which some of them are purchased from specific companies and some were custermized in lab. In this chapter, the commonly used setup for both cell sorting and micromixer projects is described in detail.

3.1 Working Solutions

The solutions chosen in this work have been used extensively in studying microfluidic chips and flow visualization. The details of working solution in this work will be presented below.

3.1.1 Buffer Solution

A buffer is a solution characterized by the ability to resist changes in pH. In chemistry and bio analysis, Most of analyzed samples are sensitive to the surrounding pH value, thus a constant ambient pH level is required. However the electrolysis of water that occurs under electroosmotic flow operation can alter the solution pH during long operating times (Bello 1996). For microfluidic applications, the surface charge present at the solid-liquid interface is also dependent on the pH; therefore, the electroosmotic mobility of the fluid also varies with pH. Addition of a buffer solution in these cases is essential in maintaining constant pH values of the solutions under investigation.

The working aqueous buffer solution used in this work is sodium (bi-) carbonate. $7.96x10^{-3}$ mol of sodium carbonate and $0.68x10^{-3}$ mol of sodium bicarbonate were added to 200 *ml* de-ionized water to create a 50 *mM* solution concentration with pH = 9.0 (Sinton 2003) The properties of the solution are similar to water: density = 998 kg/m^3, viscosity, μ = 0.001 kg/m^2, and thermal conductivity, k = 0.6 W/mK. These values are used for modeling the buffer solution.

3.1.2 Fluorescent Bye

Fluorescent dye is used in flow visualization to aid the imaging of specific regions of flow that are difficult to observe with bright-field illumination and direct monitoring methods. Choices of the dyes implemented in the fluid system are important to the overall effectiveness of the fluorescent visualization methods. The fluorescent dye was placed in the sample reservoir and used to visualize sample focusing. The dye used in this study is standard reference fluorescein (Molecular Probes, Oregon) diluted in 50 *mM* sodium (bi-)carbonate buffer to a concentration of 100 μM. Fluorescein has a peak excitation frequency of 490 *nm* and a peak emission frequency of 513 nm. The absorption and emission spectra are shown in Figure 3-1. The concentration of the dye solution is low enough so that fluid properties can be assumed to be the same as the electrolyte buffer. The diffusion coefficient of fluorescein at this concentration has been reported to be 4.37 x 10-10 m^2/s and the dye is anionic (Sinton 2003).

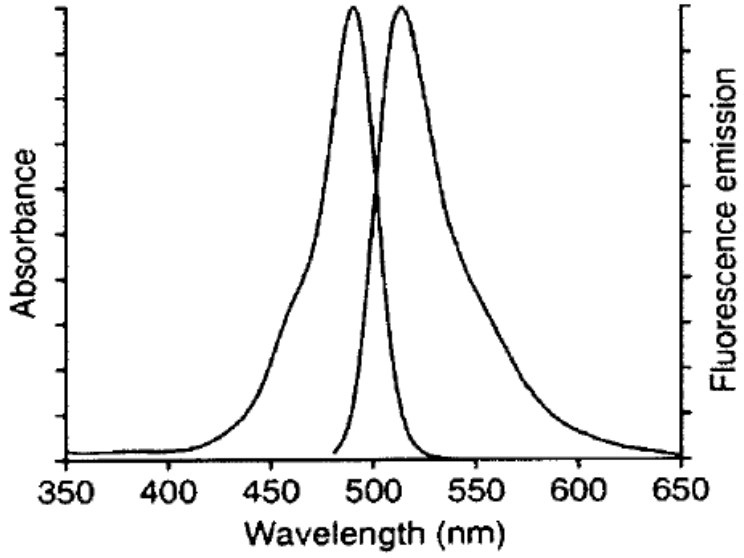

Figure 3-1 Absorption (left) and emission (right) spectra of fluorescein

3.1.3 Fluorescent Particles

Fluorescent particles used in this work are 4.0*um*, 3.8 *um* and 1.0 *um* in diameters. The beads are made from a polystyrene latex material with a sulfate modified surface and they are filled with a fluorescent dye mixture. The concentration of the stock particle solution is 2% or 5.7 x 10^8 *particles/ml*, but was diluted to 0.05% for experiments. Properties of the particles are not well reported, but the sulfate modified surface groups are believed to produce a negatively charged surface. The peak excitation and emission wavelengths for the yellow-green particles are 505 nm and 515 nm, respectively. The second set purchased from Polysciences, Inc. (Pennsylvania) consists of microspheres with a nominal diameter of 1.0 μm and are reported to be neutral or slightly negatively charged (Eckenrode, Jen et al. 2005). The stock solution has a concentration of 2.5% or 4.55 x 1010 *particles/ml*. A diluted sample concentration of 0.025% was used in experiments. The 1.0 μm particles are also yellow-green fluorescent and have peak emission and excitation wavelengths at 441 nm and 486 nm, respectively. The third microparticle solution has spheres with a nominal diameter of 3.8 μm and was supplied in a 0.005% aqueous solution, approximately 1 x 10^7 *particles/ml* (Bangs Laboratories, Inc., Indiana). These particles contain a combination of dyes and can be excited with any light in the range of 365 *nm*-650 *nm*.

3.1.4 Buffer Oxide Etch (BOE) for Fibre

BOE is aqueous NH4-HF Etchant Solutions and consisted of NH4 30 - 50%, HF 0.5 - 10% and water 40 - 70%. This solution is extremely dangerous due to its poison and strong corrosive.

BOE may etch glass but not high density polystyrene, so it can etch fibre cladding layer and core. But etching should be done in fume hood with ventilation on. All the containers for etching fibre and waste are made of polystyrene.

3.1.5 Preparation of Solutions

50*mM* buffer solution is stored at 2-5 ^oC . Before using, it is filtered with 0.2*um* filter. To maintain the same pH value, fluorescent dye sample and particles are diluted to the desired

concentration with buffer solution and stored at 2 to 5 ^{o}C . However, since fluorescent dye and particles form suspension solution, shaking of the solution is required before using it.

The BOE is a stock solution and requires no dilution or mixing with other chemicals. The 5*ml* BOE has been shown to be capable of etching a fibre for several times in thisour work before it is replaced by fresh BOE solution.

3.2 Flow Control

To drive fluid in microchannel, external power input is required. So far the widely adopted approaches are electroosmosis-driven (EOF) or pressure-driven flow. Pressure-driven flow is employed widely for macroscopic engineering while EOF is common for chemistry and bio-analysis.

For EOF, a high power supply is necessary to construct electrical field which drag ions in fluid. In this work the electrical field for EOF flow and pressure-driven flow are achieved by a power sequencer HVS-488 3000 and a syringe pump Model '11' Plus (HARVARD APPARATUS) respectively.

3.2.1 HVS488 3000 Power Sequencer

HVS 488 3000 device provides eight coordinated channels of high voltage sourcing and sensing, each capable of supplying a maximum of 3000 V. The eight channels enable as many as eight reservoirs to be designed in the fluidic chip for controlling the fluid transport.

A powerful sequencing environment coming with sequencer allows the channel levels to be changed manually in real-time or programmed for more complex sequences. The ability to control the voltage is necessary for focusing and cell sorting studies. Current and voltage monitoring during experiments provides authentication of the applied potential field and helps in the discovery of system irregularities, which generally indicates disconnected electrodes or the presence of bubbles in the channels.

The software has been provided by Labsmith to control the HV sequencer from Labview to automatically set the voltage distributions.

HVS sequencer programming in Labview enables automatic operation without any interaction. To implement sequencer programming in Labview, Labview driver should be installed in the computer which control HVS sequencer. Before sequencer programming, it is necessary to check if all channels are working properly. Any broken channels may automatically stop sequencer. For broken channels, they have to be disabled to avoid disruption to the sequencer.

3.2.2 Flow Switching

With EOF, flow direction may be controlled through changing the electrical field. In automatically operation mode where electrical field has response time as fast as optical speed, but the bottleneck that limits the frequency of flow switching is communication between computer and sequencer, computer itself characteristic, among others.

To reach a steady state voltage, 60-80*ms* is required as shown in **Figure 3-2**. Most contributors for response are using serial port communication. Actually as far as HVS sequencer is concerned the response time may go down to 10*us* or below.

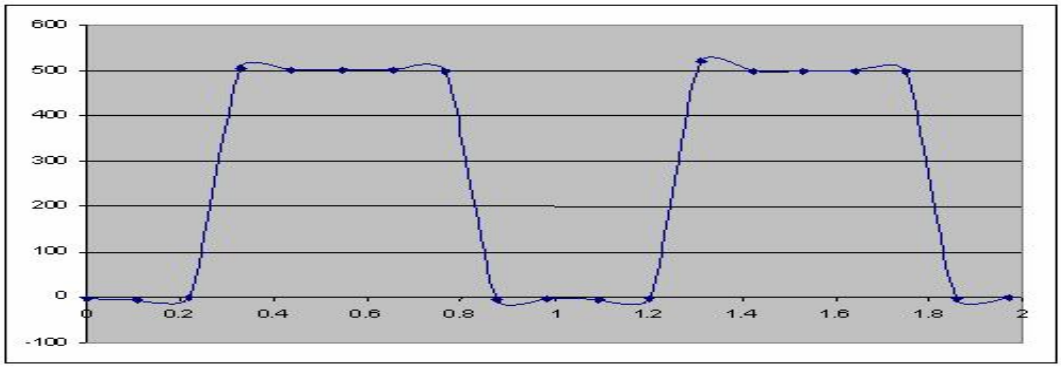

Figure 3-2 A trace of high speed channel switching is shown in Figure 9 with 100 ms intervals.

3.2.3 Syringe Pump

Model '11' Plus syringe pump (Harvard Apparatus) is designed as a low cost, single (one syringe on) or dual syringe pump capable of achieving low to moderate back pressures. The syringe pump can be set to infusion or siphon mode by switching the button on the back of pump which changes pump movement direction. All the settings can be entered through thin film buttons on front panel. With 50/60 *cc* syringes, the maximum 8 *p.s.i.* pressure may be output and 100 *p.s.i.* for 1 *ml* syringe.

Calibrating syringe pump must be done to cater to the tiny amount of fluid involves working with microchip. With 5 *cc* BD syringe, the accurate diameter 11.58 *mm* is calibrated.

As the two syringes are constructed together, independent control of each pump is impossible. To have two different pumps, two different syringes (in diameter) are required.

The special connector (Upchurch Scientific and Mcmaster-Carr) is used to connect pump to chip. The connector is glued on the chip with silicon after or before bonding. While attaching the connector on the chip, inserting a similar size syringe tip in the reservoir hole may avoid silicon leaking in reservoirs. Between the pump and connector a soft tubing (UW Chem Store) is used. The size of the tubing is determined by the syringe tips. Trapped air bubble in connector is the most common problem. To reduce this problem, extra care has to be taken to drive the air out of the syringe and the tubing when the syringe pump is connected to the chips.

3.3 Fluorescent Microscopy

3.3.1 Microscope

There are two microscopes used in this work: Olympus GX-71 reflected light inverted microscope (Figure 3-3) and Olympus BX-51M (Figure 3-4). GX-71 is used for micromixing experiment because the light source and objectives illuminate the chip from bottom. For the micromixing, pressure pump has to be connected on the chip so there is no clearance on the top. For the cell sorting experiment, as the final design uses silicon wafer as the substrate,, the light

source has to be shinning on chip from the top as the silicon substrate is not transparent for light to pass through. Both microscopes have CCD camera mounted on it to take images. Using the software Image Pro-Plus, we can measure channel width, light intensity across channel and generate movie and so on.

Objective lens is very important when the local feature is investigated. However at higher magnifications, less amount of light is gathered by microscope. Different objectives come with both microscopes so that many tasks can be done with the microscope. The list of objectives is as the following:

Table 3-1 Objective specifications for BX-51M and GX-71 fluorescence microscopes

Objectives BX-51M	**UMPlanFI-BD 10x**	**UMPlanFI-BD 20x**	**UMPlanFI-BD 50x**		
Magnification	10x	20x	50x		
NA	0.3	0.4	0.5		
Working distance(mm)	6.5	3	10.6		
Objectives GX-71	**UMPlanFI-BD 5x**	**UMPlanFI-BD 10x**	**UMPlanFI-BD 20x**	**UMPlanFI-BD 50x**	**UMPlanFI-BD 100x**
Magnification	5x	10x	20x	50x	100x
NA	0.15	0.3	0.46	0.5	0.8
Working distance(mm)	12	6.5	3	10.6	3.3

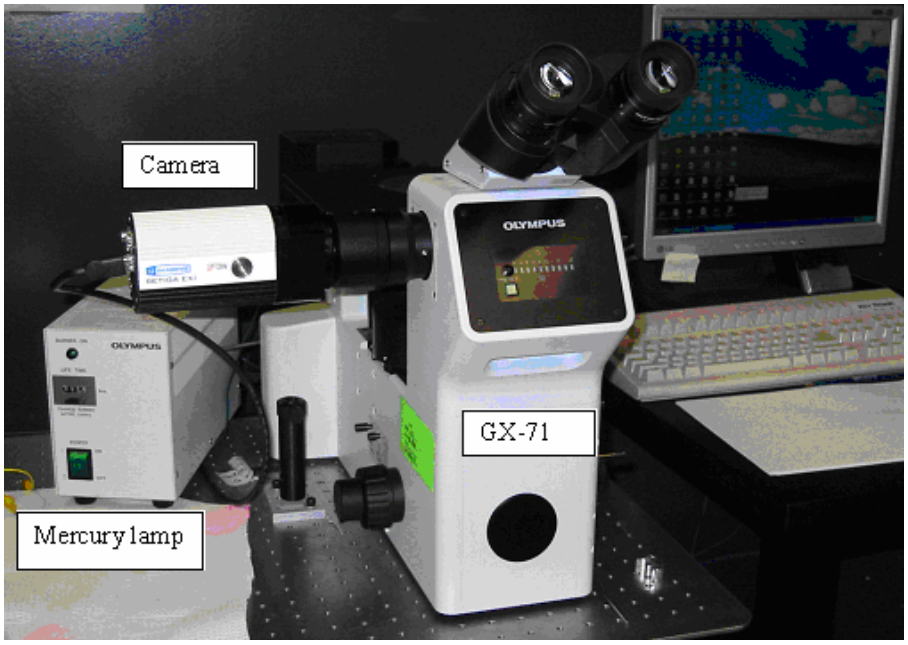

Figure 3-3 Olympus GX-71 inverted microscope. The whole system includes CCD camera, microscope, halogen, mercury lamp and filter

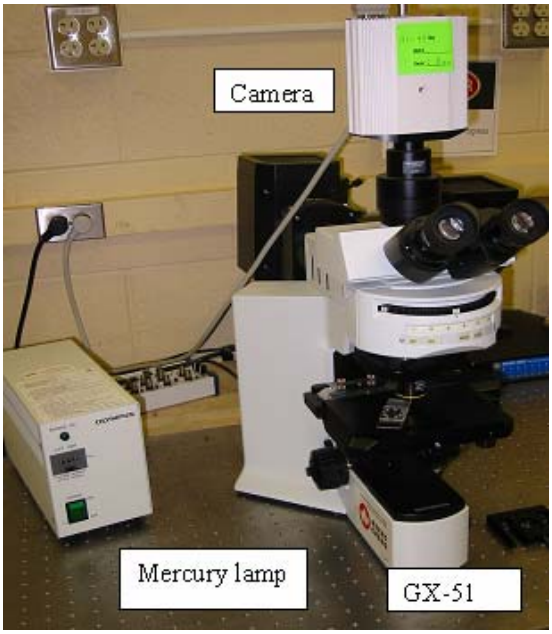

Figure 3-4 Olympus BX-51M microscope. The whole system includes CCD camera, microscope, halogen, mercury lamp and filter

3.3.2 CCD Camera

The CCD camera is used to record high speed images during microscopy visualization. The key specifications for a CCD camera include the frame grabbing rate, the spatial resolution, the sensitivity, and the scan recording technique. High frame rates are desirable to capture sequences and perform particle tracing. The monochrome CCD camera used in this work (Photometrics CoolSNAP ES) can acquire images at 10 frames per second in full-scale and full-depth operating conditions. The merging of neighboring pixels, called binning, allows up to 50 frames per second at full-depth. The CCD sensor has 6.45 x 6.45 μm pixels with an imaging area of 8.77 x 6.6 mm and a 12 bit image depth to quantify both low and high level signals in the same image. The camera has high quantum efficiency which allows sensitive observation under low light conditions. The CCD uses a progressive scan imaging process which acquires signals from all pixels sequentially during one scan. This differs from interlaced scanning which scans only the odd pixels or only the even pixels during each scan. Progressive scanning eliminates flickering that can occur with interlaced scans and provides better resolution.

The camera is mounted to the BX-51M microscope with a 1.0x magnification c-mount adapter. The approximate field of view corresponding to the 10x, 20x, and 50x objectives are 880 x 660 μm, 440 x 330 μm, and 180 x 130 μm, respectively. Calibrations were performed for each objective using images of a micrometer scale.

A similar camera (Q-Imaging Retiga EXi Mono) is used in visualization with the GX-71 microscope. This camera acquires images at 12 bit depth with pixels of the same size. The frame rate and scanning method are the same as the CoolSNAP ES. A 0.5x c-mount provides a wider field of view than the BX-51M system. Calibrations were completed for all of the objectives using the same micrometer scale procedure.

Image Pro-Plus is the software used with both systems to capture the images and perform post-image processing. Intensity line profiling, particle tracing, data filtering, image level adjusting, and spatial measuring were commonly executed in Image Pro-Plus. For acquisition, the program is very flexible and has several manual and automatic adjustment features.

3.4 Safety Considerations

As with all experimental work, precautions must be taken to ensure safety. Neither the chemical or mechanical aspects of this work present uncommon hazards. Some optical and electrical aspects, however, are noteworthy.

3.4.1 Laser Safety

In this work, a class 3B Argon air-cooled ion laser 35 LAP 321 with 40mW power output is used. Alignment is performed to make sure that the laser is working under the desired power output. Prior to laser alignment, Inspector from laser safety office would come to lab and to make sure that all precautions have been taken. For users of the laser equipment, they are required to attend the video course on laser safety provided by the University of Waterloo.

3.4.2 Chemical Handling

Several chemicals employed throughout experiment are potentially hazardous to the health of the user. The most dangerous chemicals and materials are the SU-8 developer PGMEA, SU-8 photoresist, acetone, PDMS releasing agent (TCMS), sulfuric acid, and sodium hydroxide, BOE. Safety measures were followed as described in their respective material safety data sheets.

3.4.3 Electrical Safety

To generate EOF flow, the high voltage is applied to each reservoir. For the microfluidic chips tested in this study, voltages up to 2000 V were applied. At such magnitude, the voltage is capable of causing physical harm to the user. However, such potential danger is unlikely as the electroosmotic flow is a low-current application with typical maximum current values ranging from 100 μA to 1000 μA. Physical sensitivity to current begins at approximately 0.2 mA with a startle reaction threshold at 0.5 mA(Greenwald 1991). At 10 mA paralysis of afflicted muscles can occur, providing a much more dangerous scenario. Asphyxia, the contraction of chest muscles that interfere with breathing, can occur at 35 mA and 50 mA is sufficient for shocks longer than two seconds to disrupt proper functioning of the heart (Greenwald 1991).

The power sequencer has a built-in current limit that is set to 6.5 *mA* and is rarely exceeded during the experimentation. Additional measures are taken to reduce the risk of electric shocks. The power supplies were grounded to a nearby receptacle. Electrical connections were covered with electrical tape wherever possible. Efficient space was incorporated into the design of the chip/electrode mount to prevent the microscope objectives from touching the platinum electrodes.

Chapter 4 Microfluidic Sorting and Counting

As stated in chapter 2, microfluidic sorting and counting devices have similar functions as the bench top cytometry. They are sample focusing, detection and separation.

The focusing may be achieved by squeezing sample flow with two side flows. In this way, 2-D focusing may be formed. Because the current fabrication technique using soft lithography in lab usually generates planar pattern, 3-D focusing is a big challenge.

Switching the voltage in the reservoirs may change the direction of the flow so that the sample flow can be directed to the targeted reservoir.

To develop the automatic portable microfluidic sorting and counting devices, the detection system become the core of the whole devices. This chapter just deals with the focusing and flow switching. Detection will be discussed in the next chapter.

4.1 Methodology

An automated sorting and counting system is shown in Figure 4-1 and close view of the chip is illustrated in Figure 4-2. The cell sorting and counting chip includes two main functions. One is hydro- focusing, the other flow directing.

Two shield flows restrict the sample flow in very narrow area close to the diameter of particles or cells which can line up particles or cells. The hydro-focusing by this configuration is only in two dimensions, not three dimensions. That means the particles may proceed up and down in sample flow. Flow directing is to guide the targeted particles or cells into the collecting reservoir and decrease the amount of targeted particles leaking into the waste reservoir.

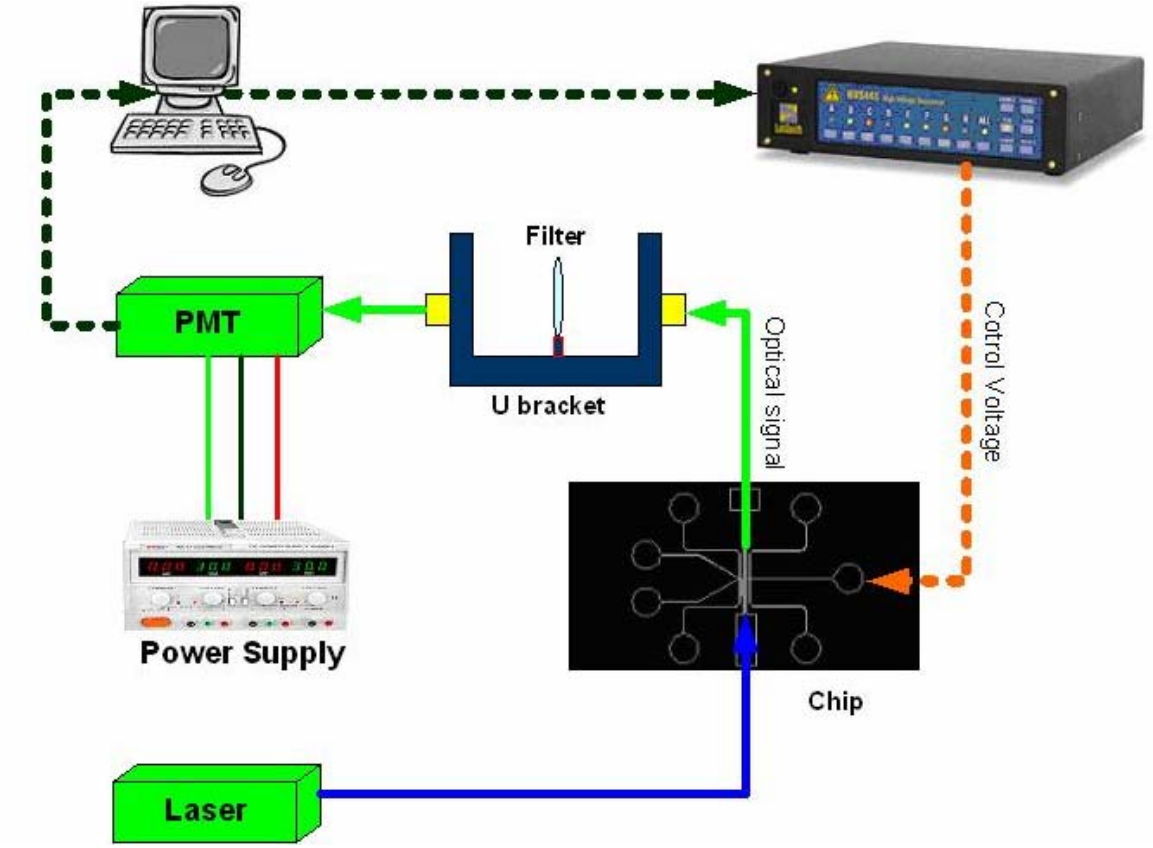

Figure 4-1 schematic of automatic cell sorting and counting

Because EOF pump has a quick response time and generates the plug-like profile of the velocity, it is employed. When the particles of interest pass the detection point, fluorescent signal may be taken by collecting waveguide or fibre and then fed into computer through the PMT which converts optical signal into electrical one. The distance from the detection point to switching section is known. If the velocity of particle can be acquired, so the time when the particle arrives at the switch section can be calculated. The control signal issued by computer to the power sequencer is used to active the flow switch so that the targeted particles will be directed into the collecting reservoir

The whole system is controlled by a software programmed using Labview. When the chip is running, laser is always shone on the channel to activate particles or dyed cells in channel through detection point. Simultaneously, fluorescent light signal picked up by receiving fibre is

propagated to Photomultiplier tubes (PMT) where optical signal is converted into electrical one. Electrical signal is further fed into the Computer through A/D card (PCI E6251, NI). Based on the signal fed into computer, the corresponding command is issued by High power sequencer which applies voltage to the electrodes.

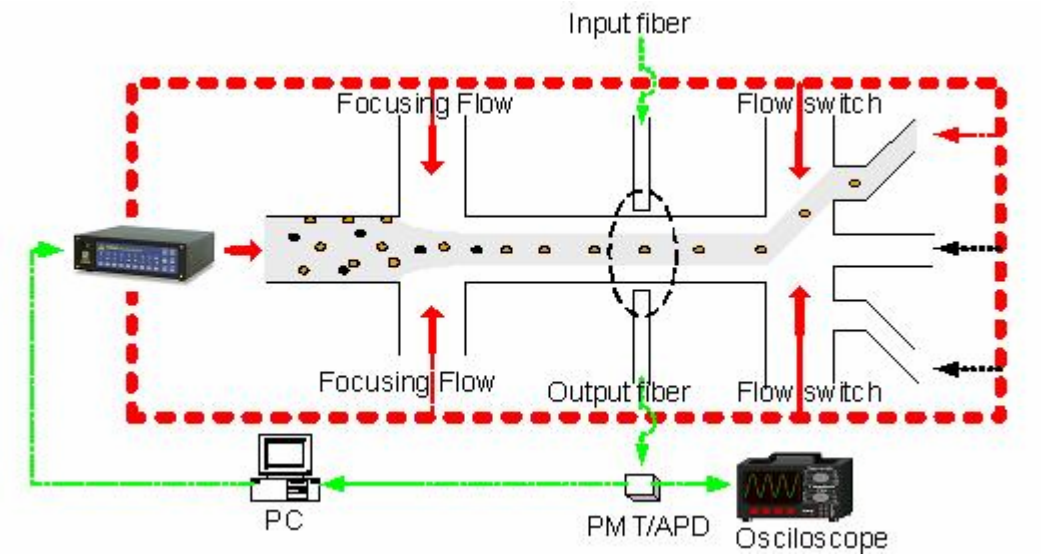

Figure 4-2 Close view of cell sorting chip integrated optical detection

4.2 Electrokinetic Focusing

Laminar flow offers us possibility to squeeze the middle flow using both side flows, which are called focusing. To detect particles or real cells in sample flow, it is expected to line up particles or real cells and force them go through detection point one by one. Detection of the particles would be difficult without focusing because they will congregate together.

As depicted in Figure 4-2, the common way to focus a sample flow is shown. In theory, the width of sample flow depends of the relative flow rate between focusing flow and sample. By applying the mass conservation law and impressible property of liquid, the model can be derived. (Yang, Chang et al. 2005) provided one model based on cross microchannel. This model was adapted and improved through numerical analysis and experiments by (Taylor 2007). Considering the applied electrical potential as low as possible and a sufficient sample flow rate, the optimized

ratio of the width of the side channel to the sample channel is 3 to 1. More detail will be provided by (Taylor 2007) .

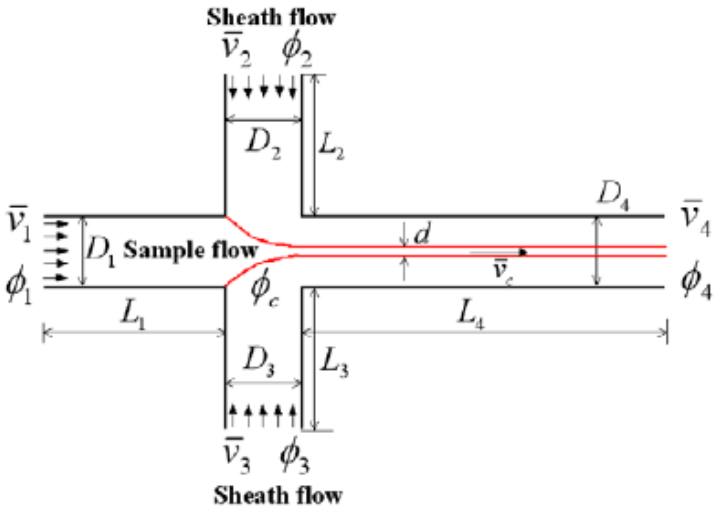

Figure 4-3 Schematic presentation for focusing model

According to Figure 4-3, the focusing model was given by (Taylor 2007) as the following:

$$\frac{d}{W_4} = [\,2(\frac{\phi_2 - \phi_j}{\phi_1 - \phi_j}\frac{L_1}{L_2}\frac{W_2}{W_1}) + 1\,]^{-1} \qquad \textbf{4-1}$$

From 4-1, the width of the sample can go down to zero. However as to have a reasonable capability of sorting and counting, the flow rate should be higher than the specific one. Normally, the width is dependent on the size of real cells or particles in the sample flow. In this work, the 4 um particles are used to validate the chips, so the width of the sample flow should be 4 um or a little higher after focusing. Considering the sample concentration and sorting efficiency, the minimum voltage for each reservoir can be determined.

4.3 Implement Hydro-Resistance Components in Chip

In Chapter 2, hydro-resistance component has been employed to limit pressure-driven flow and it is more efficiency to reduce the height of channel than the width. However the minimum fabricated height of channel and particle size, whichever is the bigger, place the limit. The cell size such as yeast, bacteria is around 4 *um*. The minimum fabricated feature in lab is going down to the 10um or a little lower.

When the EOF flow is required, the undesired pressure-induced flow has to be avoided. Considering the case in this work, the height of the main channel is 30 (width) x 55 (height) *um* with and without hydro-resistance. To reduce the effect of flow expansion or contraction from the wide/narrow channel to the narrow/wide channel, the same cross section area is used to ensure the same flow rate. Pressure drop along channel is kept the same; finally it can be shown that:

Q (without hydro-resistance element)/Q (with hydro-resistance element)

= (30x55^3)/(165x10^3)=30.25

It is apparent that the hydro-resistance elements can suppress most of pressure-induce flow. However challenges are faced when trying to incorporate the hydro-resistance elements as multilayer chip is necessary to have channels of different depths. Firstly, multilayer chip is not easier to fabricate than single layer which does not need alignment. Secondly, contamination of multilayer fabrication is more likely to occur than that in single layer.

Without hydro-resistance elements on the chip, it is very hard to have a stable focusing flow; the focusing flow is either offset from the center of channel or disturbed when solution is being loaded. With hydro-resistance elements on the chip, the focusing flow is hardly disturbed due to a little difference of hydrostatic head, even for loading solution. By loading fluorescent solution into the cross channel chip with or without the hydro-resistance, the hydro resistance is investigated.

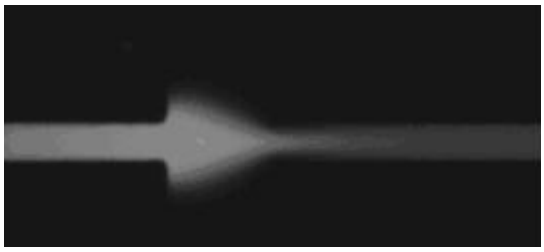

Figure 4-4 Focusing investigation with fluorescent dye. After focusing intersection. The fluorescent dye is focused almost at the center of the channel.

4.4 Flow Switching

Analogous to electric currency, the direction of EOF flow can be reversed by switching the voltage applied to the ends of channel. In this way, no removable parts such as valves are required.

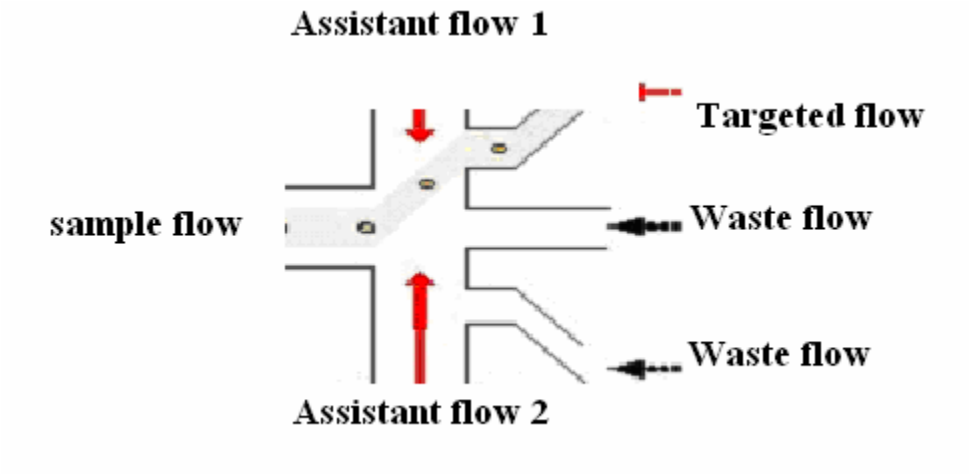

Figure 4-5 Flow switching with two assistant flows

The structure of the simplest flow switching is without tow assistant flows. Just switching the voltage between the target flow and waster flow, the sample flow may be directed from waste flow to targeted flow. However the leaking was observed. Two assistant flows may reduce sample flow leaking so that the efficiency of sorting can be increased.

4.5 Chip Holder

During experiments, the cell sorting chip is mounted on chip holder as shown in Figure 4-6. Chip holder can hold testing chip in place and distributing the electrical potential into each reservoir. As discussed earlier, electrode location will induce Laplace pressure because the different location of electrode in reservoir forms a different meniscus between liquid and air. To avoid as much induced pressure as possible, the electrode is placed at the center of the reservoir and sample has the same level. After chip is mounted and electrodes are placed in the reservoirs, the relative positions are maintained during experiment so that the undesired pressure can be reduced. Using chip holder may reduce the part of pressure, but not remove to the expected magnitude.

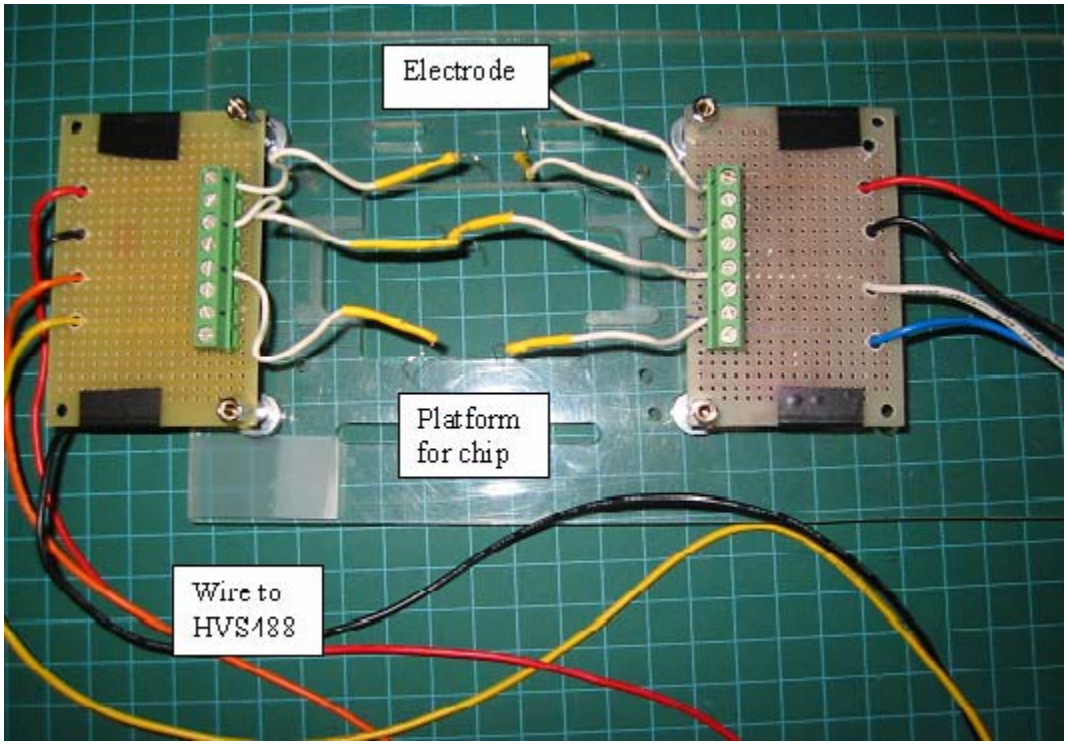

Figure 4-6 Customized Home-made Chip Holder for mounting chip in place and distributing electrical potential

Chapter 5 Optical Detection for Microfluidic sorting and Counting Devices

In this chapter, optical detection, the core part of microfluidic sorting and counting devices will be evaluated through experiments. Reliable and sensitive optical detection can make portable microfluidic sorting and counting devices more robust.

Embedded fibers can guide laser beam close to the sample in the channel and lead to less power loss compared to shinning laser directly on the channel. For multi-point optical detection, it is not physical to employ embedded fibers. So integrated beam splitters and waveguides in the microchip offer possible opportunities. As well-known, to guide light in the waveguide, the refractive index of the waveguide should be higher than that of the surrounding. PDMS does not work for this purpose. Hence a hybrid chip PDMS-SU8-Silicon wafer chip is proposed and evaluated. The details about experimental setup and designs are discussed.

5.1 Optical-Mechanical-Electrical Aspects

5.1.1 Fibre

Basically, fibre has a structure as shown in Figure 5-1. From center to outside the fibre consists of a core which guide light, a cladding layer which wraps outside of core tightly to support core and a buffer layer which is normally plastic to support and protect the core and the cladding layer. The refraction index for cladding layer is lower than core so that fibre can direct light in it due to total internal reflection.

Normally, cladding layer of the fibre available on market is 125um and buffer layer is 250um. The core diameter depends on that it is single or multi mode fibre. Single mode fibre has core diameter below 9 um; multi mode one has core diameter above 9um. Most of features in microchips have a channel height below 100um since the spin coating can not guarantee the patterns above 100um very well. In most cases in this work, the channel height is around 50um. This means fibre has to be etched down below 50um for it to be fitted in the channel.

Fibre core and cladding layer are made of glass and thus very stable; strong and often corrosivechemicals are required to etch it. One commonly used chemical is HF solution (Aqueous NH4-HF Etchant Solutions, Mallinckrodt Baker, Inc). Before etching fibre, the jacket layer which loosely wraps outside of buffer layer should be removed using fibre stripper (Model MS-4B-E Micro- electronics, INC.). After jacket removal, the plastic buffer layer is exposed. This plastic layer is resistant to HF solution can thus needs to be removed using the fibre stripper.

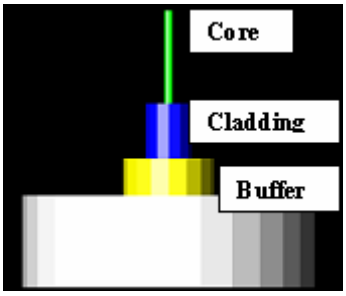

Figure 5-1 Fibre structure. Green is core, Blue is cladding layer, yellow buffer layer and white jacket.

According to the supplier, the approximate etch rates of 6:1 BOE on SiO2 at the corresponding temperatures are:

- 25C ~ 1000 A/min (~0.100 μm/min)
- 35C ~ 1700 A/min (~0.170 μm/min)
- 45C ~ 2400 A/min (~0.240 μm/min)

The amount of cladding material that is etched can be calculated if the duration of etching is known $\Delta t = \frac{Dia_{Initial} - Dia_{Final}}{2 \times etch\ rate}$. The etching process should be monitored regularly as to prevent over-etching the layer. In this work, it takes six hours to etch fibre down to 50um or smaller.

After etching, fibre end should be cut by a standard fibre cutter to obtain a flat end.However most of the cleavers available on market are not for cutting standard fibre with a125*um* thick cladding layer. In our case, the cutting is achieved using a diamond scrapper.

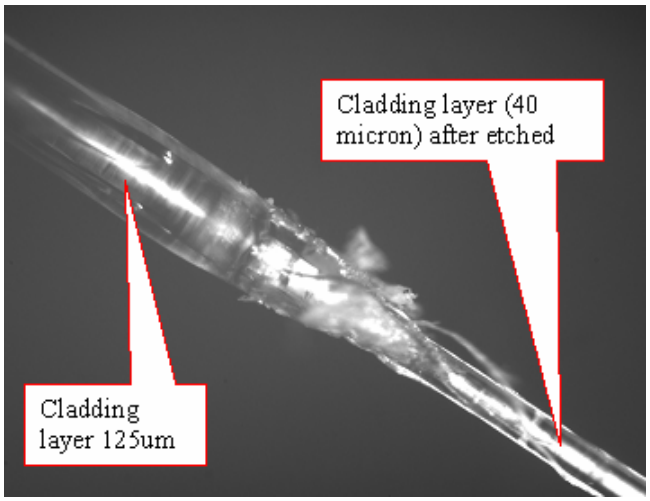

Figure 5-2 Etched fibre. It has definitely different segments. The left was not etched, the right was etched.

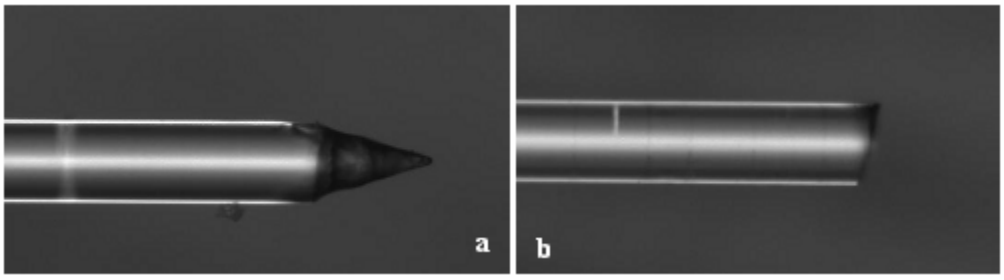

Figure 5-3 Etched fibre. (a) Before cutting the end (b) after cutting the end. Comparing (a) with (b), even though the end is cut, the flat end is hard to get due to no special fibre cleaver can do this.

5.1.2 Laser

In this work, Argon air-cooled ion laser 35 LAP 321 is chosen and shown as Figure 5-4. The excitation wavelength of the fluorescent dye chosen in this thesis is 488*nm* and emission wavelength is 515 um with a total power of 150*mW*.

The laser comes with separate power supply. Alignment was carried out to install a coupler on the laser head so that the fibre can be fixed to the laser machine. This is done by first coupling fibre

to the coupler mounting on laser head and leaving the other end of the fibre to be connected to a photodetector that measures the power from the fibre. If the fibre is successfully attached to the coupler and yet no light is detected, it is the most possible that no laser beam comes out from laser. A simple method is to put a screen right before the free end of fibre. The light is very weak which may not be sensed by photodetector. Now this can be solved by adjusting the tilt screws on coupler to allow more light to pass through. Alignment is done when most of light is guided by the fibre and detected by the photodetector. Regular maintenance and re-alignment are needed to make sure that the alignment is always in place.

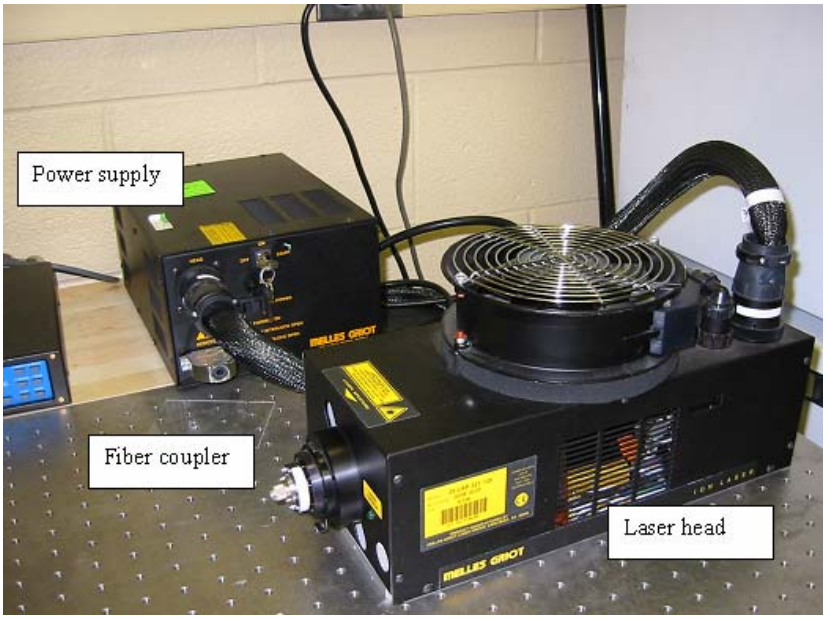

Figure 5-4 Argon air-cooled ion laser 35 LAP 321. When the laser is running, the enough clearance around laser head is necessary.

5.1.3 Photomultiplier Tube (PMT) and Power Supply

In microfluidics, fluorescent (FL) dye is commonly used to investigate the flow in a microchannel. However the signal emitted by FL is so low that most of common instruments could not pick it up. This requires either PMT (H9656-02, HAMAMATSU) or APD which is ideal to detect very weak light signal. Both instruments are very sensitive and are able to count individual photons.

Referring to Figure 5-7, two modes can be used to adjust PMT sensitivity; one is voltage programming, the other resistance programming. Relatively resistance programming is simpler and only one variable resistance is needed. A power supply of $\pm 15V$ is needed for PMT and GPS-4253 with 4 output channels will be ideal in this case. In our experiments, it was observed that grounding GPS-4253 is necessary.

PMT is very susceptible to damage during shipping and storage. Hence simple testing should be performed to check its functionality. Testing setup is shown in Figure 5-5. The PMT and the filter are placed in a black box. The laser power should be set to minimum first and then increased gradually to avoid damaging PMT. A working PMT should give the black curve shown in Figure 5-6. On the other hand, a defective PMT will give small signal close to the dark current signal (red curve).

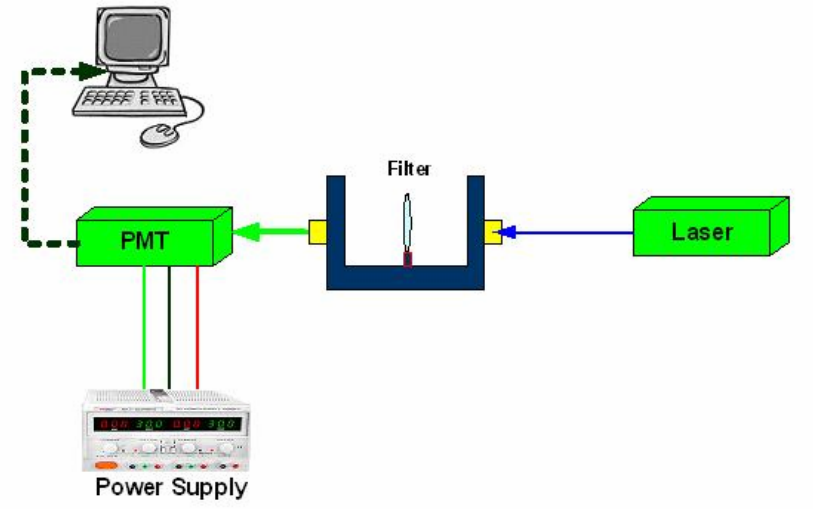

Figure 5-5 PMT and filter testing configuration

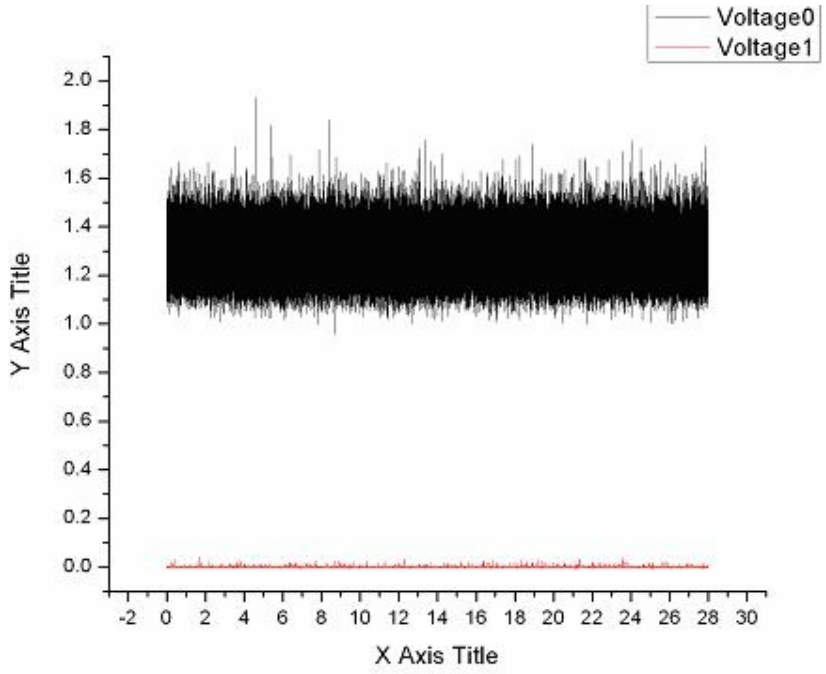

Figure 5-6 Testing signal of PMT. When testing, one PMT is connected to the signal, the other just dark current signal (red curve).

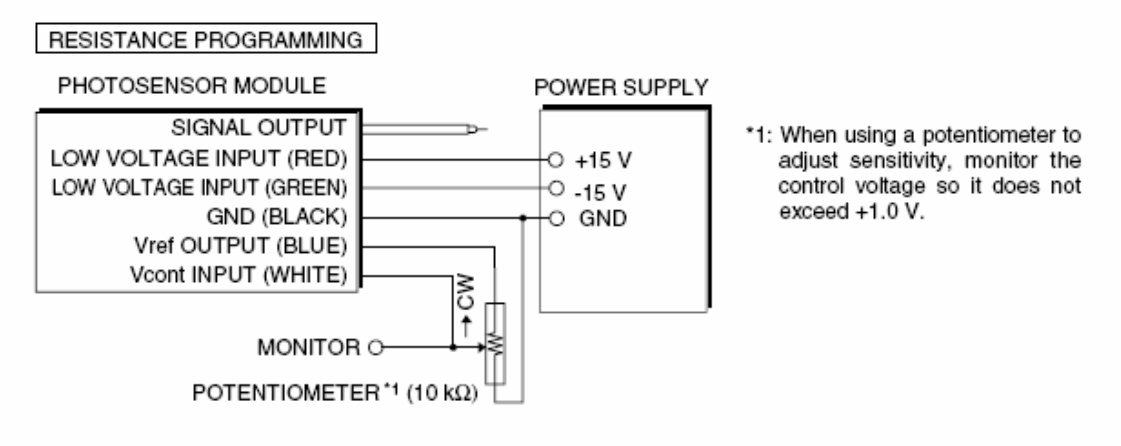

Figure 5-7 PMT Wiring with Resistance programming

5.1.4 Filter Lenses and Holder

Because of difference between the excitation and emission wavelength, a filter lenses is necessary to remove excitation and background noise. Considering emission wavelength peaking at 515nm, several band pass filters which cover 515nm are selected to compare their performance. In this work, 525/50nm, 530/40nm (Chroma Technology Corp) filter lenses were chosen. All the filters are 12.5mm diameter and mounted on filter holder OAH 0.5in and mount stage (Siskiyou).

As shown in Figure 5-5, a U-bracket (UB-02-33-550-M-M-1.80, OZ OPTICS) with coupler on is needed in order to guide light signal to filter and then feed it to PMT through fibre. Each side of U-bracket has a coupler for the fibre. Alignment and adjustment in this case was carried out by manufacturer.

A home-made base machined in school work-shop is used to mount U-bracket and filter holder. The relative position between U-bracket and filter holder affects the signal. To reduce signal loss, filter should be adjusted perpendicular to the line between the couplers of U-bracket.

5.1.5 Signal Processing and Software

The whole system is controlled by Labview program. Considering compatibility, data acquisition card NI PCI-6251 is chosen for easy-use with software. To bridge PMT and NI PCI-6251 together, NI BNC-2120 adapter is installed.

5.2 Design I - Embedded Optical Fibre for Detection

As light experiences the natural diffraction during propagation, a light cone can be generated. Design 1 utilises this phenomenon. Only one light source is used to excite certain range along the sample channel.

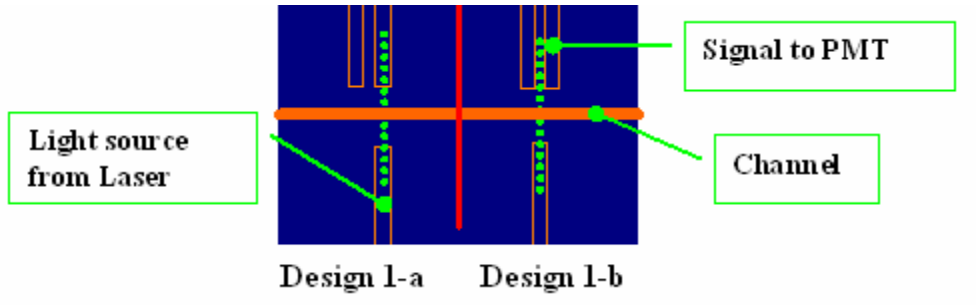

Figure 5-8 the designs of PDMS chips with two configurations of embedded fibre.

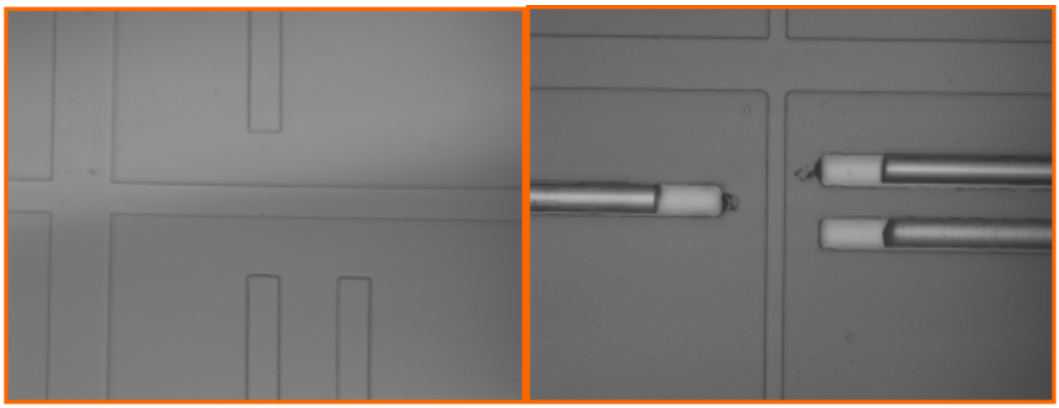

Figure 5-9 PDMS chips for Embedded fibre detection. The left is Design 1-a, the right is the design 1 –b with fibre in.

For PDMS chip with embedded fibre, two configurations are designed and evaluated. A glass substrate is used and the distance from the fibre channel to the sample channel is 50 *um*. This chip is multi-layers with a sample channel of 25 *um*, and fibre channel 55 *u*m. In this work, the focusing is 2-D, so the particles or cells in the sample flow after focusing move forward up and down in the sample flow in the vertical direction. The fluctuations of the particles in the sample flow may affect detection accuracy. At the same time, the channel may be blocked if the channel is to shallow. In my case, 25 *um* is much bigger than the particles or common cells and blocking is not likely. The original fibre has a diameter 125 um; removing the buffer layer and the subsequent etching can reduce the diameter to 50um without significant degradation in quality. The 55 *um* fibre channel is a little higher than the etched fibre to guarantee fibre insertion.

Under the microscope, the fibre is inserted into fibre channel. To facilitate insertion, the liquid PDMS is used as a lubricant. At first, liquid PDMS is dropped at the mouth of the fibre channel after bonding of PDMS to substrate. The liquid PDMS is driven into the fibre channel by capillary force. Then the etched fibre is inserted with care. After insertion, the whole chip is left alone at room temperature for two days to have liquid PDMS cured. A fast way is put the chip into oven or on the hotplate to promote curing of the liquid PDMS in fibre channel. In the latter, it was observed that the fibre is pulled away from the sample channel a little bit because the jacket of fibre has the different expansion coefficient from the core and cladding layer. Thus it is recommended that the curing liquid PDMS in fibre channel should be conducted at the room temperature.

For design 1-a, the fibre is right opposite to one of the two receiving fibres. When the fluorescent particle pass the detection point, only one fibre right opposite to the excitation fibre can pick up signal. The other collects only the noise. For design 1-b, two receiving fibres did not pick up signal. The possible reason is the most power is at the center of the light cone.

Looking back at these designs, at least four fibres need to be used to detect the signal as reported by (Xiang, Xuan et al. 2005). However incorporation of many fibres leads to not only the increase in the cost, but also the system complexity.

5.3 Design II - Integrated Optical Components for Detection

5.3.1 Optical Waveguide

Analogous to water in a pipe, light can be guided in waveguide. Normally, to achieve guiding of light, the waveguide needs to have a higher refractive index than the surrounding. The wavelength of light is in the order of nanometer so it is sensitive to any defects present in the waveguide is bigger than the wavelength of light as they will lead to radiation loss. Physically, part of light is lost to the surrounding in the form of heat. Optical fibre is also working under this principle total internal reflection.

Light propagation is governed by the Maxwell equation. The general form of Maxwell equations is the frequency-domain form(Vassallo 1991):

$$\nabla \times E = -i\omega\mu_0 (H + M)$$

$$\nabla \times H = i\omega(\varepsilon_0 E + P) \qquad \textbf{5-1}$$

Where E and H are respectively the electric and the magnetic field at (circular) frequency ω, P and M are the electric and magnetic polarisation densities respective; μ_0 and ε_0 are the vacuum permittivity and permeability.

Based on the model above, numerical analysis can be done with the commercialized softwares, COMSOL Multiphysics, Optiwave and Mode Solution.

Optical waveguides can be classified according to their geometry (planar, strip, or fiber waveguides), mode structure (single-mode, multi-mode), refractive index distribution (step or gradient index) and material (glass, polymer, and semiconductor). The most common waveguide is fibre. It has circular cross section. However, the waveguide fabricated using Photolithography technique can give rectangular cross section.

To sort and count particles or cells, the flow has to be controlled. In other words, the velocity needs to be precisely monitored. To date most of the applictions reported employ single point detection ((Lee, Lin et al. 2003)). Under EOF flow, when the pressure-driven flow is very small thus negligible, the velocity can be calculated to predict the particles or cells location in the microfluidic device. In this work, two-point detection is proposed to measure the velocity of particles or cells. Previously, Dr. Li reported a system with two-point detection. Two fibers were embedded close to the focused sample flow, and two receiving fibers were placed oppsite to excitation fiber to collect the fluorescent signal. The particles are 15um so that weak signal was not exercised.

5.3.2 SU8 Filled Channel as Waveguide

With embedded optical fibre to enhance detection, it can not be achieved tow point detection by only one input fibre. Because of the optical properties of SU8, it naturally becomes a candidate to fabricate waveguide.

Preliminary investigation is conducted by filling SU8 into pre-fabricating channel as waveguide. In testing, it is found impossible to fabricate a complete waveguide in this way because SU8 is hydrophobic to the PDMS. Therefore the alternative approaches, SU8 chip has to be investigated. In the following segment, the design and fabrication of SU8 chip will be presented in detail.

5.3.3 Design II - SU8 Chip

SU8 is widely used in the microfluidic research to fabricate master (mold) due to its excellent optical property. It has a higher refractive index than glass and PDMS and almost transparent to visible light, thus is the best candidate for fabrication of the optical elements. To guide light, a material with lower refractive index around the SU8 optical elements is required. This is the reason why fabrication of PDMS-SU8-Silicon Hybrid chip is common. In the hybrid chip, the optical elements are fabricated in SU8 layer with PDMS at the top and silicon at the bottom and air at both sides. All the material around the SU8 optical elements has a lower refractive index so that the light can be propagated in SU8 optical elements under total internal reflection.

To achieve two-point detection with only one light source, the optical beam splitter should be needed to split the light into two. The waveguide is also needed to guide the excitation light to sample flow. Again the coupler is a very important element. Most of loss power is caused by low efficient coupler.

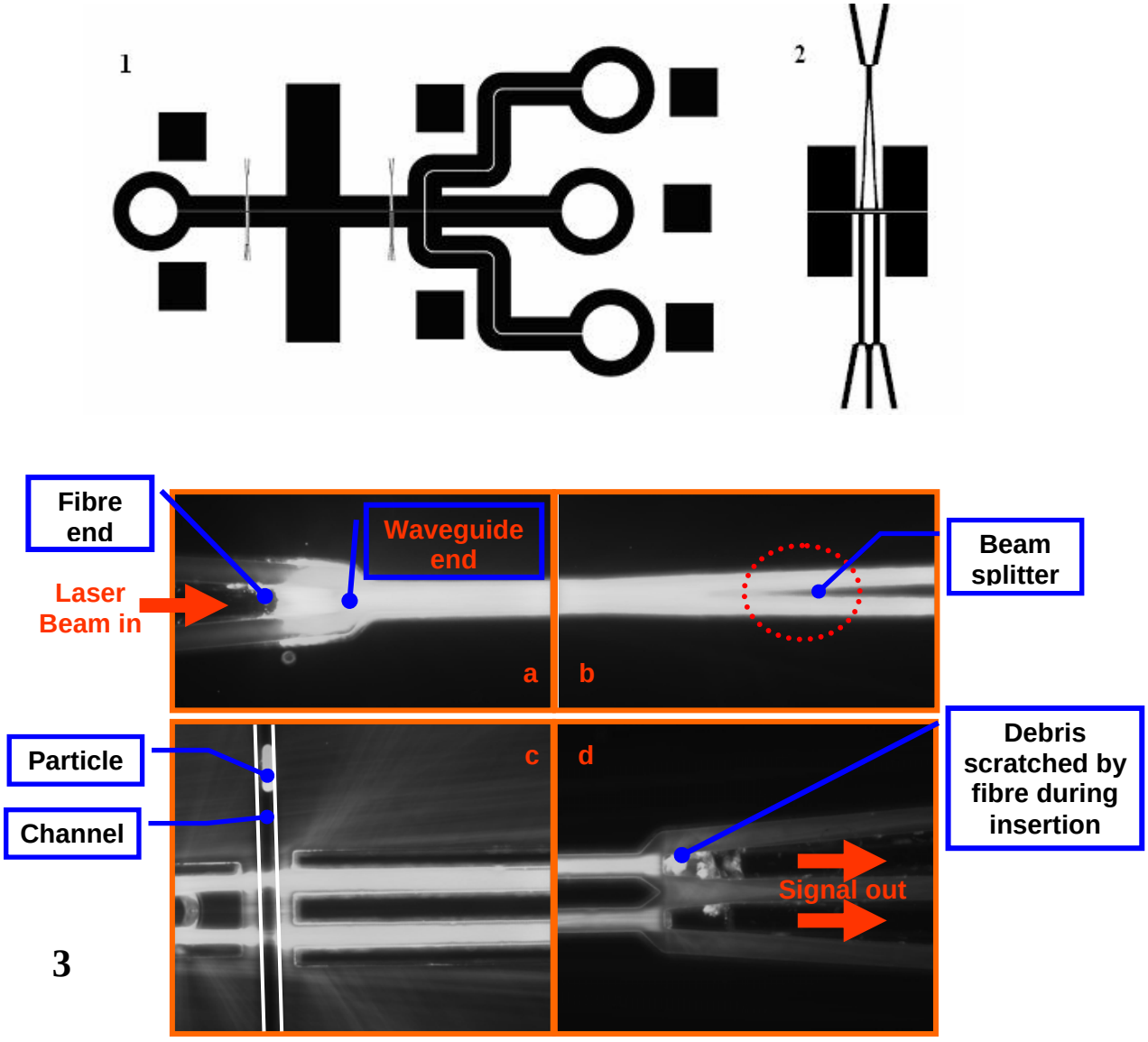

Figure 5-10 SU8 hybrid chip design II-a (1) the chip structure. (2) The close view of coupler, beam splitter and waveguide. (3) Images of integrated optical elements.

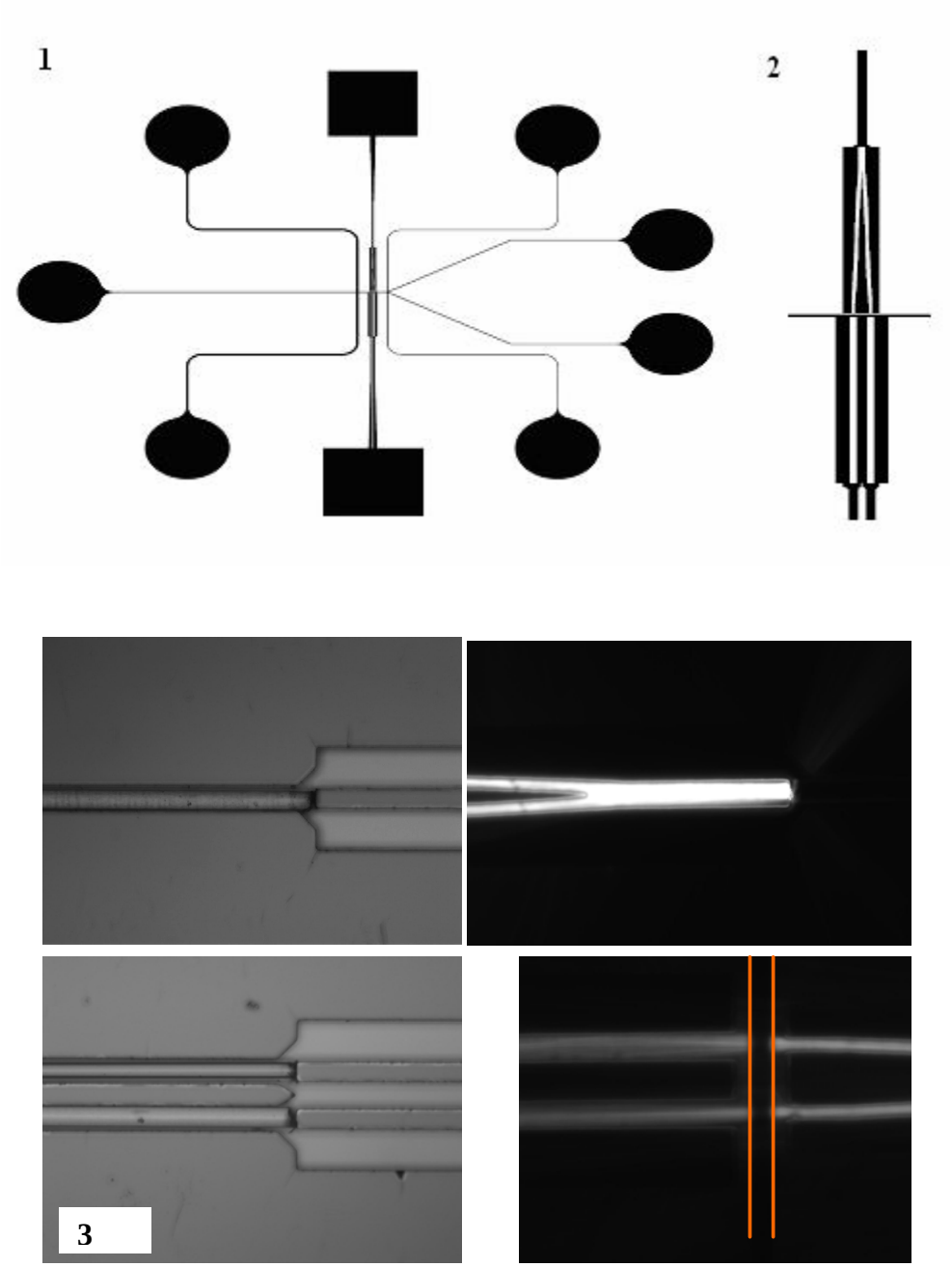

Figure 5-11 SU8 hybrid chip design II-b (1) The chip structure. (2) The close view of coupler, beam splitter and waveguide. (3) The images of integrated optical elements.

5.3.3.1 Fibre Coupler

Two kinds of the coupler are shown as Figure 5-10 and Figure 5-11.

The first design is shown in Figure 5-10. The fiber coupler has a V-groove. It has be found to be not very efficient as the fiber end could not be fixed to the end of waveguide without an efficient coupler. Leakage of light is often observed and debris is commonly observed after inserting fiber from Figure 5-10 3-d. As observed under the microscope, the wall of waveguide and channel was found to be very coarse. That is inevitable due to the scratch of SU8 during inserting fibre into coupler.

The second design Figure 5-11, the coupler is open to the end of the beam splitter. From images, the fibre can contact the end of the beam splitter after the fibre is secured using tape. No debris is found. So the second coupler is more efficient than the first one.

5.3.3.2 Optical Beam Splitter and Arcs S waveguide

For both designs, the beam splitter is a Y branch splitter which is well established in the network of telecommunication. The detail design was reported by (Ruano, Glidle et al. 2003).

Referring to the Figure 5-12:

$$L_A = \sqrt{4Rd - d^2} \qquad \textbf{5-2}$$

$$L_T = \frac{n_{eff}}{2\alpha\lambda_0}(W^2 - W_0^2)$$

To achieve losses as low as 0.1 dB, (Kawachi 1996) reported the at least 15mm radius is needed for the bending waveguide. In this work the distance between two detection points is 100um. So the unique length L_A is calculated as the following:

$$L_A = \sqrt{4 * 15 * 0.1 - 0.1^2} = 2.45mm$$

Consider the diameter of etched fibre, the end width of beam splitter to the fibre is 40um width and each waveguide after S bend is 20 um width. The taped waveguide for the beam splitter is not necessary.

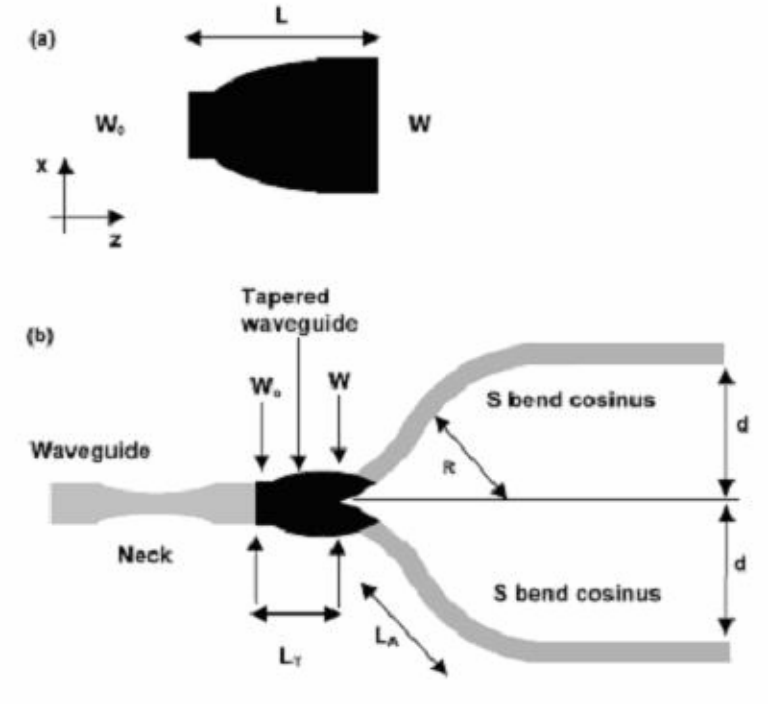

Figure 5-12 (a) Schematic representation of a tapered waveguide consisting of a waveguide with different input and output widths. (b) Schematic representation of a Y-branch, divided in three parts: a taped waveguide and two S-bend arcs. Y-branches with multimode waveguides can have a narrow neck to minimize the variations of the splitting ratio versus the lateral beam displacement

5.4 Results and Discussion

Design I fails to detect two different points with one light source and is thus abandoned.

In design II-a, the channel wall is 1mm. Along the channel after focusing section, two sets of optical elements are deployed. Firstly, the defects are observed often when coating SU8 on silicon wafer; uneven surface is often a big problem to bonding. 1mm channel wall reduces the contact surface so that the risk of bonding is expected to be low. From our experiments, this is however not the case as leaking is observed. Secondly, the fibre can be broken easily when inserted into the coupler.

Based on design II-a, the integrated optical elements are able to detect the particles in the channel in spite of some problems. After some improvement, the final design, design II-b, is shown in Figure 5-11. The leaking problem was not found in this case. In design II-b, the measured signals are shown in Figure 5-13 and Figure 5-14. As the sample solution is diluted no particles in the focused sample flow pass the detection point in parallel. To see if the integrated optical elements are working, a signal is recorded when one particle is seen to have passed the detection point using microscope. Figure 5-13 and Figure 5-14 show detection of one particle signal. It can be found out that filter 535/40 is better but the noise is still high relative to the signal. As the optical detection is symmetrical and one of two collecting waveguides can pick up a signal, the signal can be acquired at two points when two filters 535/40 are available.

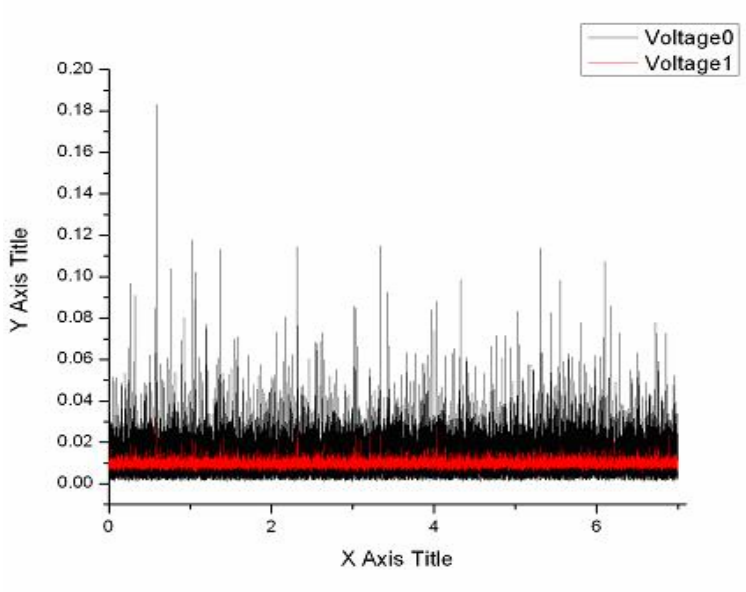

Figure 5-13 Fluorescent signal with filter 525/50nm

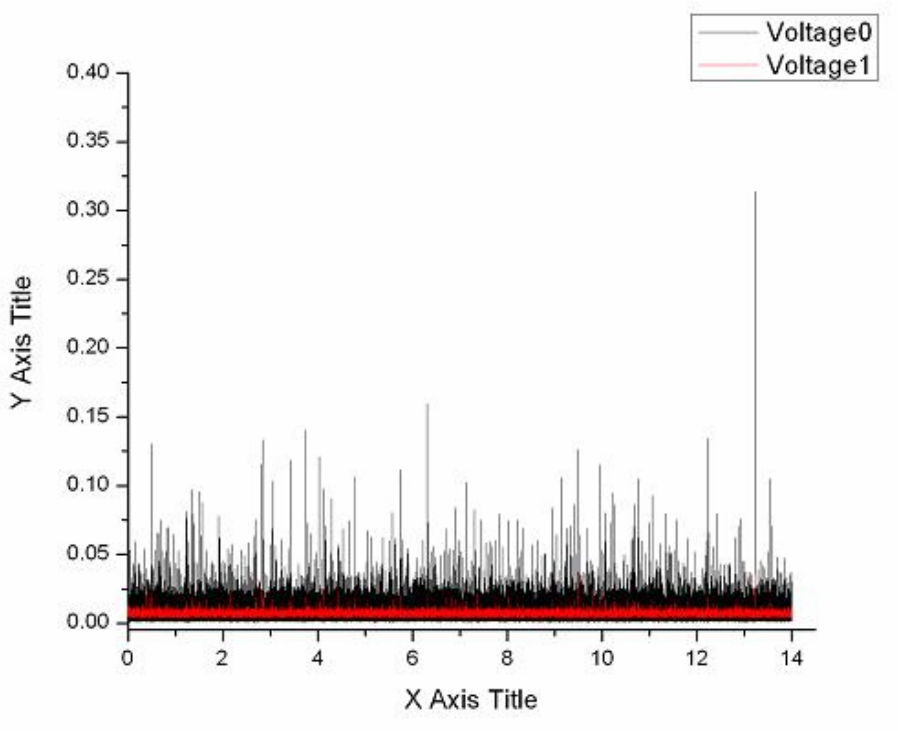

Figure 5-14 Fluorescent signal with filter 535/40nm

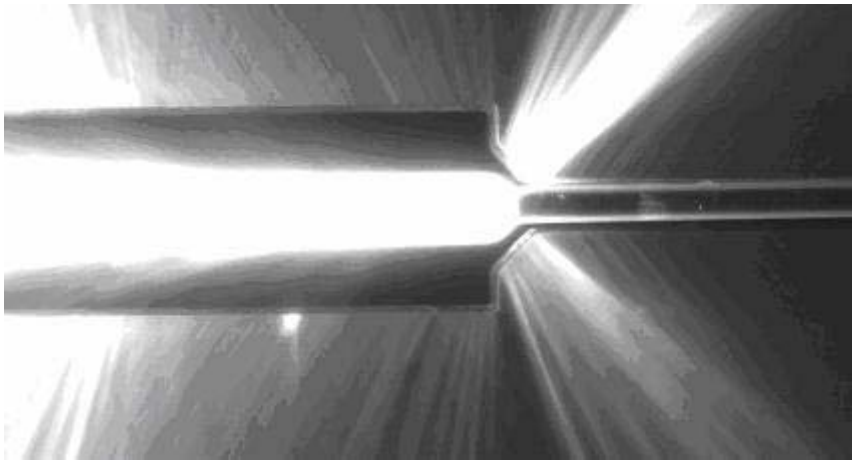

Figure 5-15 Laser shinning on waveguide at the maximum power output

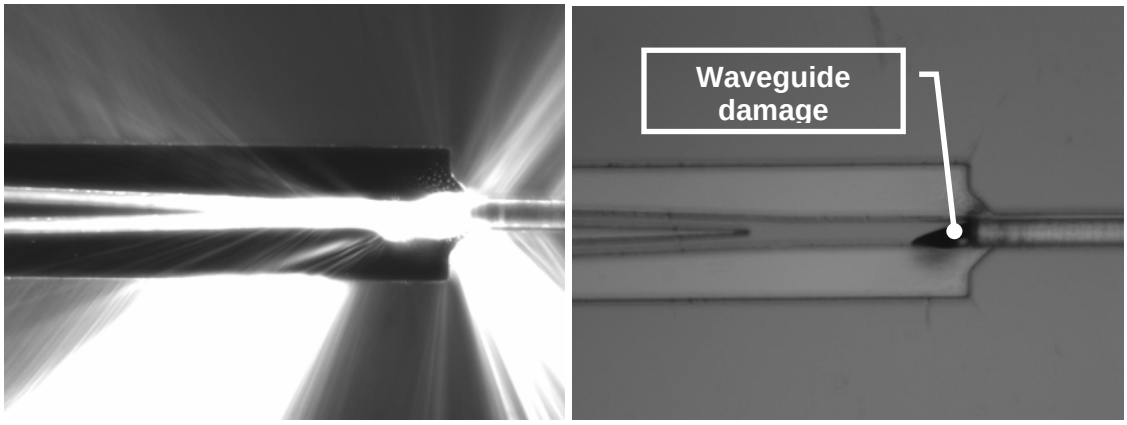

Figure 5-16 Damaged waveguide observed during experiment. The left: the damaged waveguide causes the light leaking. The right: at the interface between waveguide and fibre is damaged.

The most obvious problem is the power loss existing at the interface between fibre and beamsplitter (Figure 5-15). Secondly thermal instabilities of SU8 optical elements were found in the experiments. When laser is working under low power output (20mW), this problem is not obvious and chip is stable for long time operation. When power is increased close to 40 mW, SU8 waveguide was destroyed in 1 minute (Figure 5-16). It is recommended that when long time operation of the integrated SU8 optical elements is needed, the chosen laser power output should be set below 20mW.

Chapter 6 Micromixer

So far, three main functions of microfluidic sorting and counting devises have been discussed. But apparently, the sample was prepared outside the chip. With sample preparation outside the chip, cross contamination may happensed and the amount of the prepared sample must be much more than required. Integrated micromixers may reduce the cross contamination of the sample solution. More importantly preparing sample solution within an integrated micromixer will dramatically reduce the use of the sample solution, especially for the expensive sample solution.

To get uniform sample solution, fast mixing has to be required. But mixing in microfluidic devices is very slow due to the laminar flow in microchannels. In this chapter, the fundamentals of micromixing is investigated through numeric simulation and experiments in Y-shaped channel. The possible designs are proposed and evaluated.

6.1 Introduction of Micromixing

Most of the fluid flows in microfluidic devices are laminar because of the small Re. Mixing in LOC devices solely depends on diffusion. Due to the increasingly demand for micromixing, micromixing have received much more attention than ever (Nguyen and Wu 2005), (Hessel, Lowe et al. 2005; Nguyen and Wu 2005), (Hardt and Schonfeld 2003) and (Hessel, Hardt et al. 2003).

Due to the absence of turbulence in microfluidic devices, mixing relies solely on molecular inter-diffusion. The diffusive flux of a solution is given by the product of diffusion coefficient, the interfacial surface area and the gradient of species concentration, i.e. $D \cdot A \cdot \nabla c$. Accordingly, diffusive mixing can be optimised by maximisation of the respective constituting factors. Enhancement of the diffusion coefficient can be achieved, e.g. by an appropriate temperature rise. Similarly micromixing translates to an efficient maximisation of interfacial surface area and concentration gradient. Above all convective diffusion enhancement is commonly employed in mixing devices. For instance secondary-flow patterns superposed to the main flow or recirculation patterns within liquid plugs of segmented liquid/ liquid flows are known to be

effective mixing means. The maximum possible interfacial area generation is however related to the viscous dissipation.

Besides the Reynolds number $Re = U * d / \nu$, the Peclét number, $Pe = U * d / D$, and the Fourier number, *Fo=Tr/Tm*, are commonly used as dimensionless groups to characterise convective/diffusive problems. Here *U, d,* ν denote the average velocity, the hydraulic diameter or the transverse diffusion distance which are assumed to be of the same order of magnitude. *Tr , Tm* denote the average residence time and the diffusive mixing time, defined as *Tr =L/U* and $Tm = d^2 / D$, where L denotes the longitudinal length. In order to achieve complete mixing, the limit requires *Tm<Tr*. When the velocity is known, the rough length for mixing channel may be calculated to guide design process.

6.2 Y Channel Mixer

Numerical simulation is set up with COMSOL Multiphysics to investigate mixing fundamental in the microfluidic devices. The simple Y channel is used in numerical simulation because it is simple geometry. The conditions used for simulation is the same as those used in the experiments. Two different liquid solutions are used. One is DI water, the other fluorescent dye. The syringe pump is preferable for this work because pressure pump is working for the neutral solution without ions.

The fluorescent dye is widely used to visualize flow in bio or chemistry analysis. The emission from fluorescent dye solution may indicate the distribution of the fluorescent dye along the cross section. For the uniform distribution, the intensity of fluorescent dye should be the same along the cross section.

6.2.1 Numerical Analysis

Boundary condition:

Flow rate: $10 \mu L / minute = 10^{-9} m^3 / 60s$

Y channel dimension: 200um width, 8.8 um depth, 6cm length

Fluorescent dye solution: $100\mu M = 0.1mol/m^3$

Diffusion coefficient of $100\mu M$: $4.6 * 10^{-10}\ m^2/s$

Density $1000\ kg/m^3$

Viscosity $0.001kg \cdot m^{-1} \cdot s^{-1}$

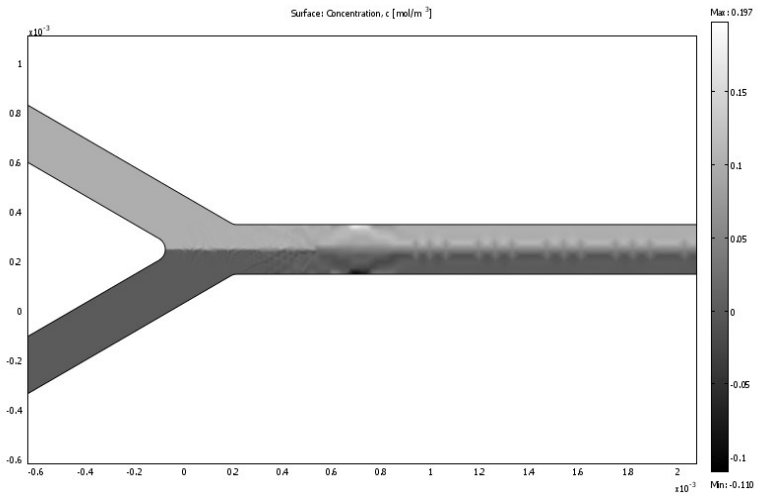

Figure 6-1 Y micromixer simulation result with COMSOL

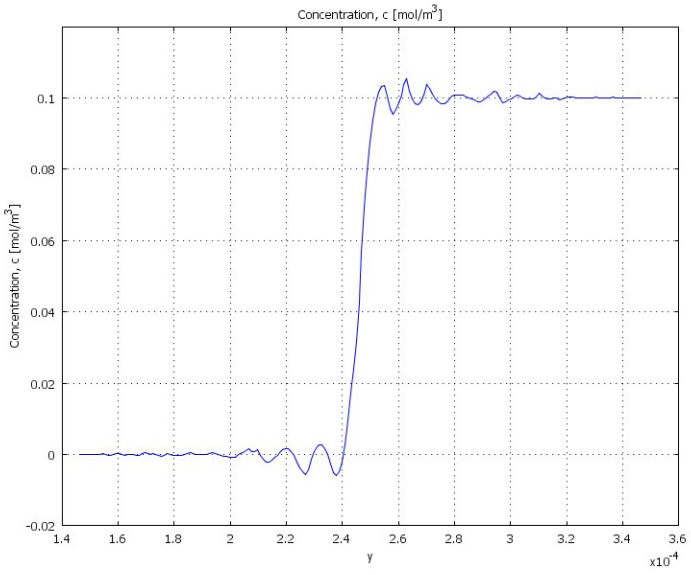

Figure 6-2 Concentration distribution at the branch of Y channel.

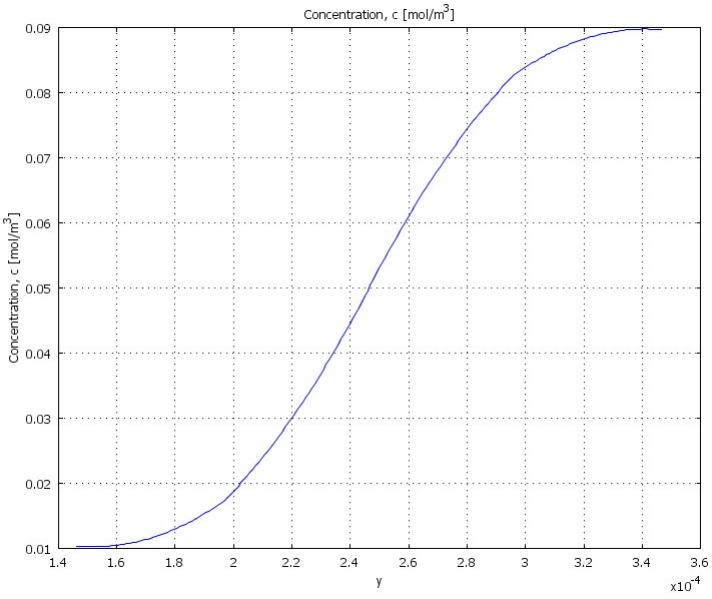

Figure 6-3 Concentration distribution at the end of Y channel.

6.2.2 Experimental evaluation

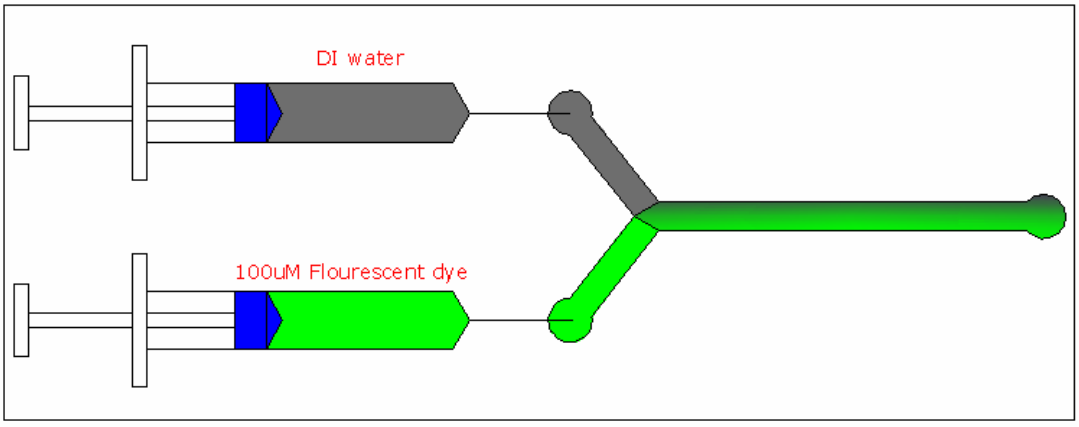

Figure 6-4 Schematic of Y channel mixing with syringe pump

Figure 6-5 **Experimental set-up of Y channel mixing with syringe pump**

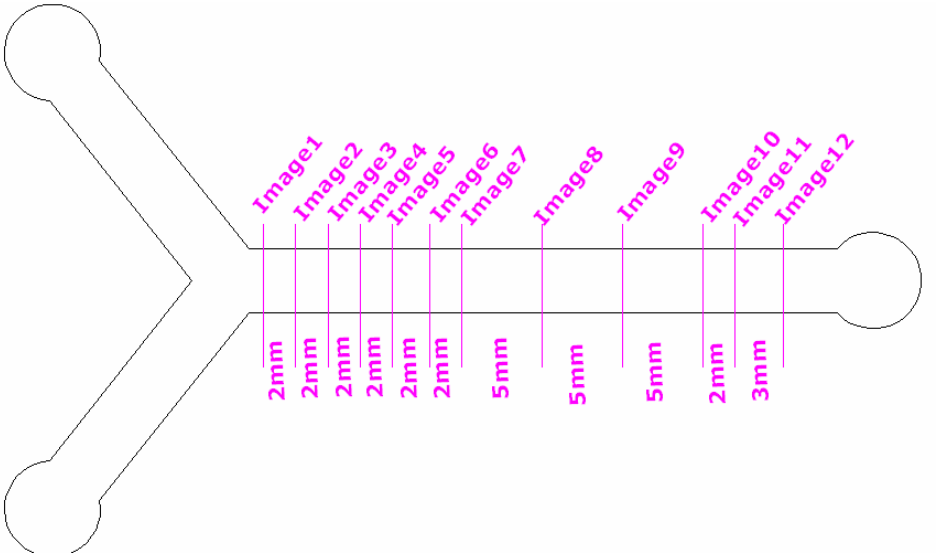

Figure 6-6 **Schematic for the location to take images along mixing channel.**

When the two flows go downstream side by side along the mixing channel, the concentration will be changing due to diffusion. This method will be used to measure the efficiency of mixing.

Syringe pump (Harvard picoplus) is employed to drive the flow. One is full of DI water, the other 100um fluorescent dye. The flow rate is *10uL/minute*.

Y Channel dimension is 200micron in width and 8.8 um in depth. To reduce noise, all the lamps in the lab are turn off during experiment except for the excitation lamp.

Images are taken at different points and the locations are shown in Figure 6-6. In total 12 images are taken. The image 12 is affected significantly by the outlet reservoir. A series of images are taken along the mixing channel and shown from Figure 6-7 to Figure 6-9.

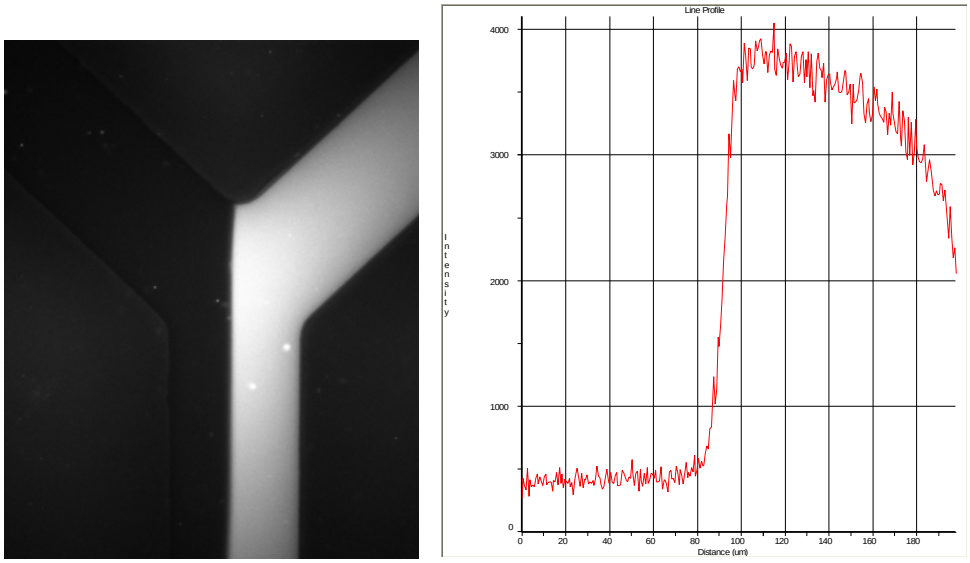

Figure 6-7 Left: image 1. Right: intensity distribution of the fluorescent dye solution

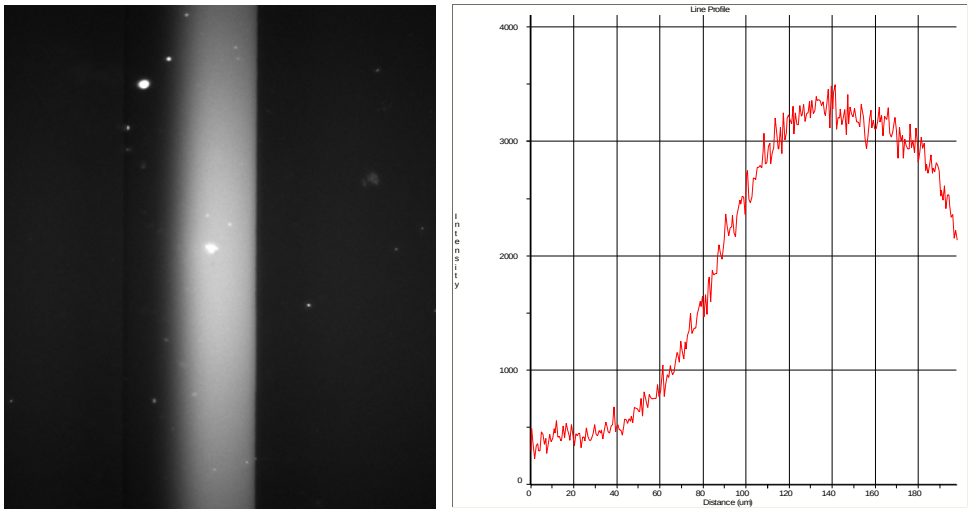

Figure 6-8 **Left: image 6. Right: intensity distribution of the fluorescent dye solution**

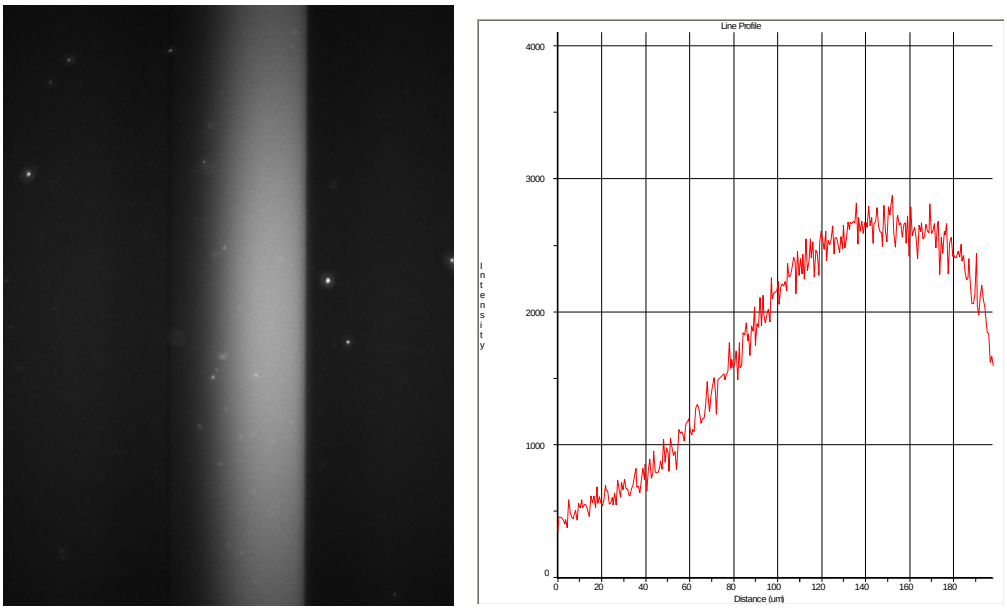

Figure 6-9 **Left: image11. Right: intensity distribution of the fluorescent dye solution**

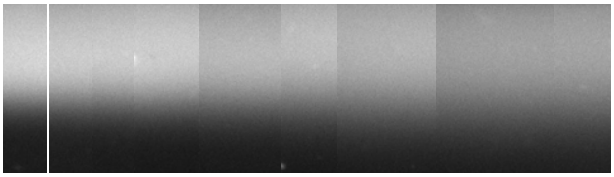

Figure 6-10 Image1 to image 9 from left to right

Comparing the results of numerical simulation with experiment, the mixing is very slow. 6 cm is not enough for complete mixing. According to the $Tm = d^2 / D$, the rough length of mixing channel can be calculated more than 30cm. For the microfluidic device it is not practical.

6.3 Interdigital Mixer

Many approaches are used to improve mixing in the microfluidic chip. For passive micromixer, the common way is to use complicated channel network to have a chaotic flow or split-recombine flow so as to have a very thin multi-laminar flow. In this work, interdigital design is proposed and evaluated by experiment. For the numerical analysis and experiment, the same conditions and solution are used. The detail design is as the following:

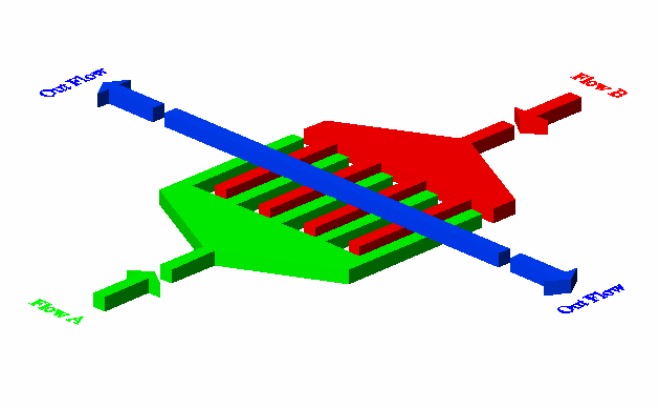

Figure 6-11 Scematic of interdigital micromixer. Blue channel: strait channel where mixing is archived. Green part is fluid A inlet channel, red part is fluid B inlet channel. The space between green and red channel is to separate fluid A and B. the arrangement of both outlets is used to get balance flow.

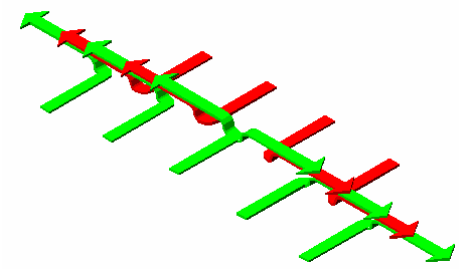

Figure 6-12 Expected flow with proposed interdigital micromer. Fluid A (Green) and B (Red) introduced from inlet channels will go up or down(depends on the strait channel arrangement) and then overlap together along strait channel flowing to the both outlets.

6.3.1 Numerical Analysis

Referring to the Figure 6-11, a simplified model is set up with COMSOL. Because the available computer resources are limit, the geometry of model has to be shrunk down. Referring to Figure 6-14, the flows are overlapped together as shown in Figure 6-12. From the simulation results, sandwich flows can be achieved. But when the strait channel is wider than the inlet channel, the sandwich flows can not be observed (Figure 6-16).

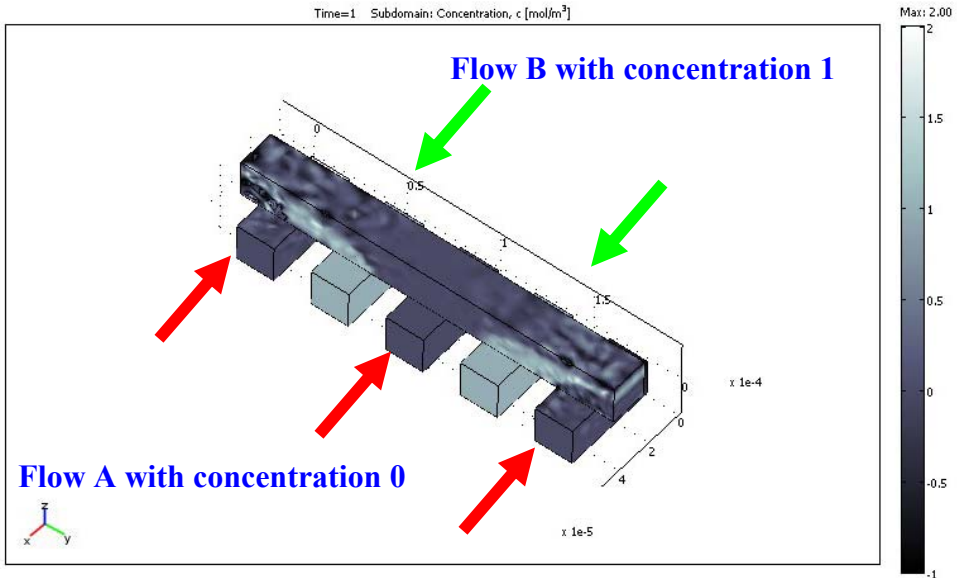

Figure 6-13 Simulation model with all channel 20 um

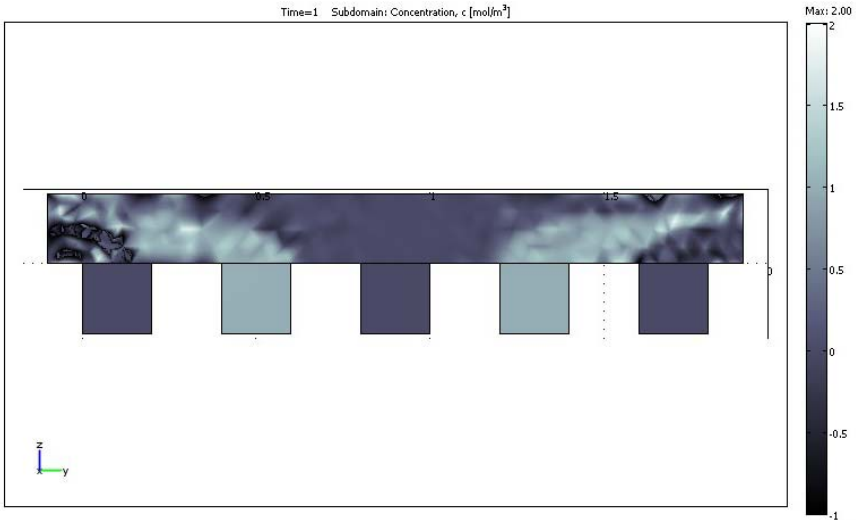

Figure 6-14 Front view of the model with 20 um channel

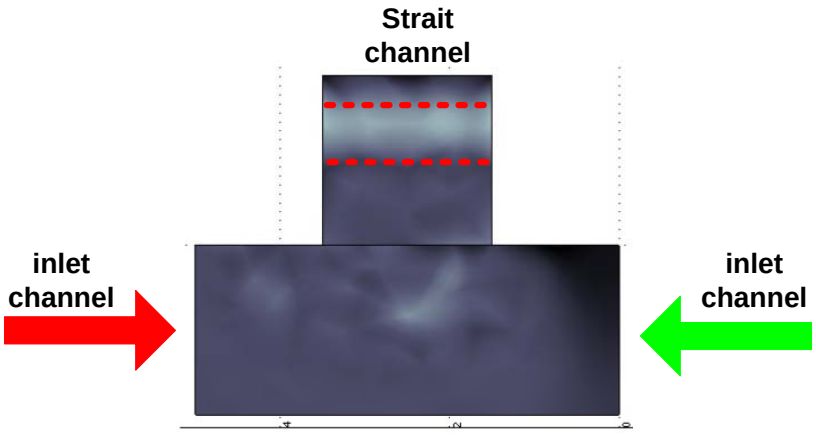

Figure 6-15 Side view of the model of 20 um channel

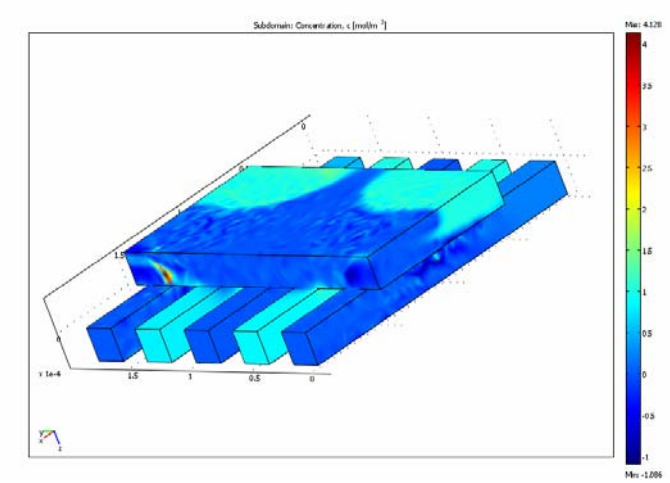

Figure 6-16 Simulation result with 100um strait channel and 20um inlet channel

6.3.2 Experimental evaluation

Based on the numerical analysis, the corresponding micromixers are designed and fabricated. This design has two layers. Bottom layer is for the inlet channel and top layer is for the strait channel. The inlet channel is 20um and100um width by 2mm length. The strait channel is 20, 100, 500, 1000um. Bonding of the inlet channel layer to the strait channel layer is to build an interdigital micromixer.

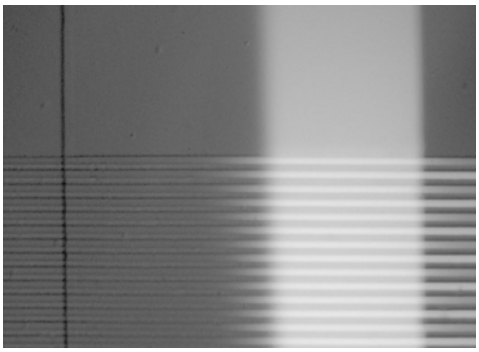

Figure 6-17 Width 20 um inlet channel by 1mm strait channel.

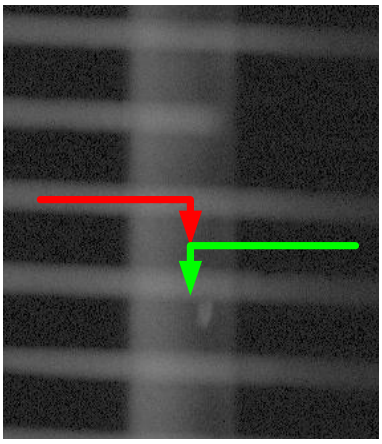

Figure 6-18 **Width 20um inlet channel by 100um strait channel**

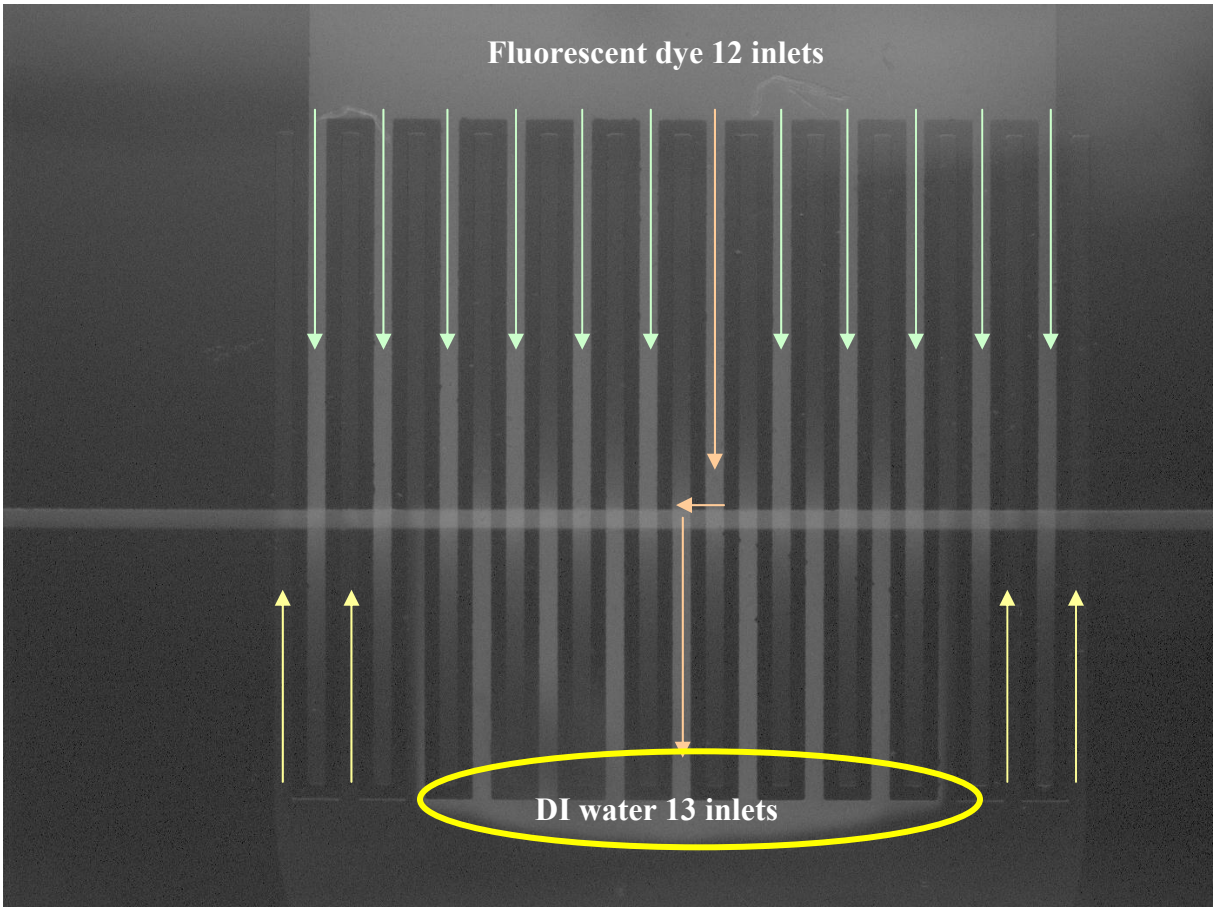

Figure 6-19 Width 100um channel for inlet and strait channel.

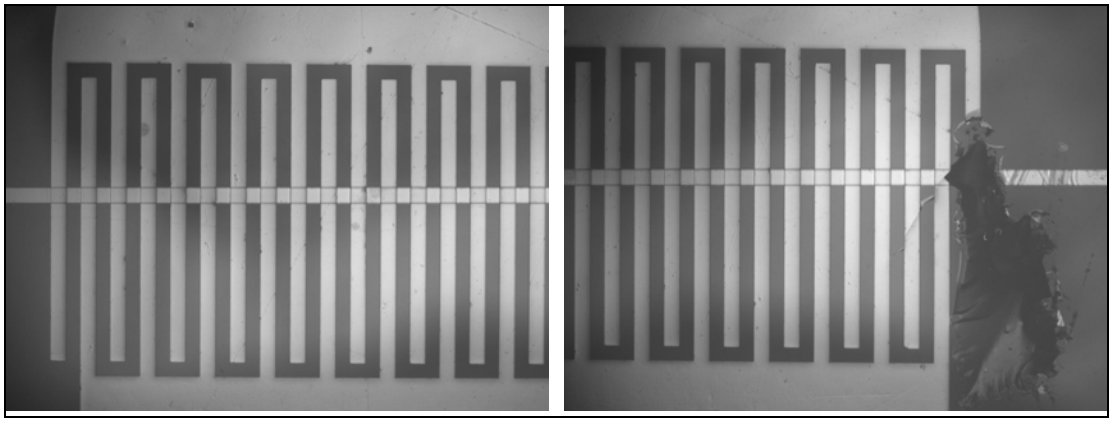

Figure 6-20 **One channel is blocked so that both inlets have the same channel 12 to 12.**

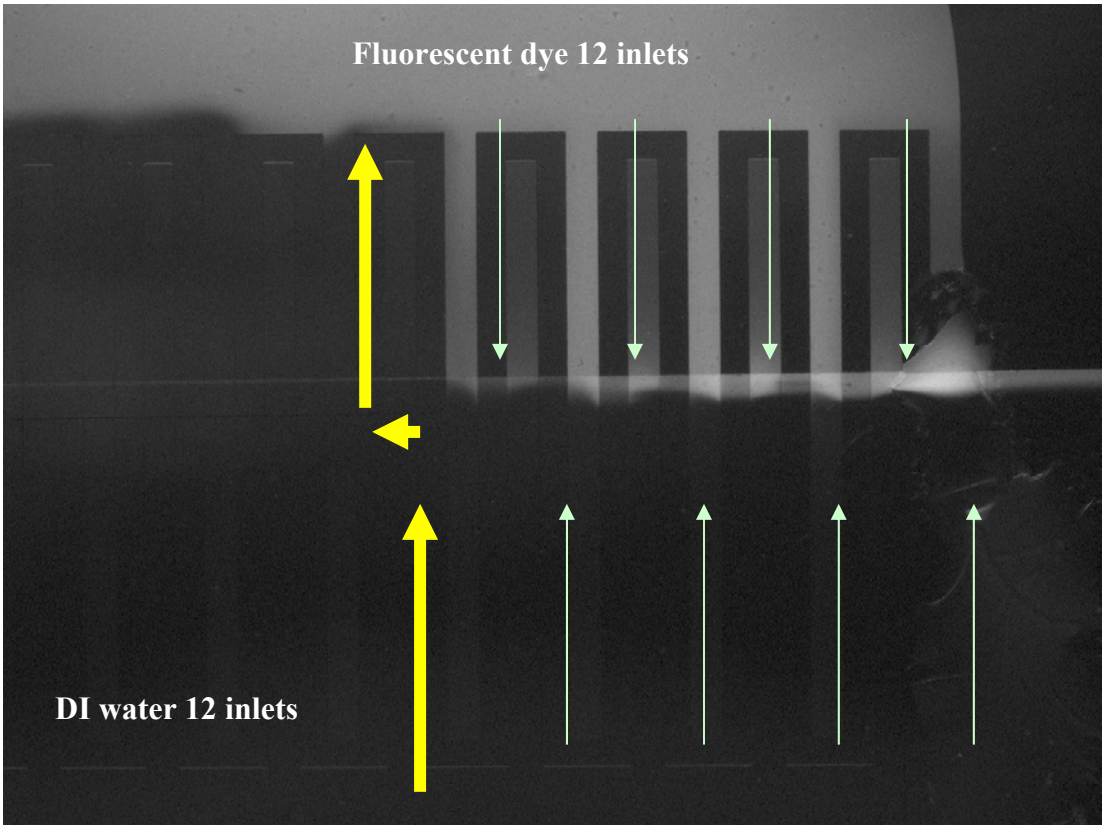

Figure 6-21 **Symmetrical inlet structure. Each side has the 12 inlet channels. Following blue path, some DI water goes to the fluorescent dye side. However, this problem is not worse than Figure 6-19**

From the Figure 6-17 and Figure 6-18, When the strait channel is bigger than inlet channel, it is easy to find the flows which are divided at the almost centerline of strait channel. That means the rear flow A cannot go over to the front of B from top, and they move on side by side. So this kind of flow can not improve mixing.

When both for the inlet and strait channel are 100um, another problem occurs. Referring to Figure 6-19, fluid flows from one side to another side. The possible reason is that there are different inlet channels for both sides. So when one channel is blocked, the remaining inlet channel will be used for both sides as shown in Figure 6-20.

Referring to Figure 6-21, after one channel is blocked, the similar problem still exists. The flows from each inlet channel have different path lengths and thus different pressure drops will be experienced. The pressure drop is very hard to balance for each inlet channel. It is related to the flow rate. The possible approach is suggested to improve this problem as Figure 6-22.

To balance the pressure drop, different lengths of the inlet channel are used so that all the inlet flows have the same path length. At the same time, the reduced length of strait channel is also suggested.

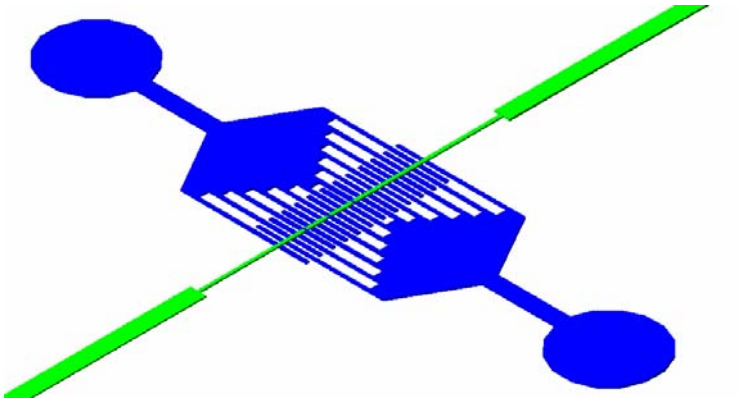

Figure 6-22 Schematic of new proposed design to balance pressure drop for each inlet channel.

6.4 Porous Mixer

Packed bed is widely used in chemical production because it provides high surface to volume ratio. It was also adopted in mixing. (Wang and Li 2007) reported a novel porous micromixer. Based on it, one bead-filled micromixer is proposed.

Beads in chamber can form porous structure as illustrated in Figure 6-23. When the distance between posts is less than the diameter of a bead, beads will not leak into working channel and pores are formed between beads. The irregular pores can split, stretch, fold and break the mixing flows and thus dramatically improves the mixing efficiency.

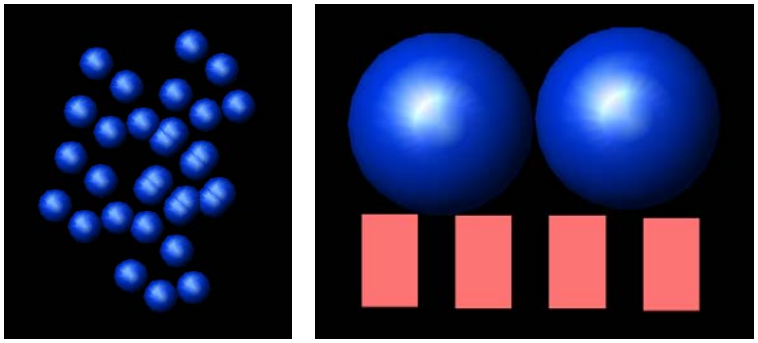

Figure 6-23 Schematic of beads in chamber. Left:Beads in chamber form irregular porous, right: beads are limited in chamber by the post in chamber.

Referring to Figure 6-24, beads may be introduced from the side channel which is then sealed or blocked. To confine bead in channel, leaking of the beads into working channel should be prevented by putting posts at the interface between chamber and working channel. The distance should be above 10um, or even up to 20um to avoid limits from mask printing resolution and fabrication. That also determines the diameter of beads which should be bigger than 20um.

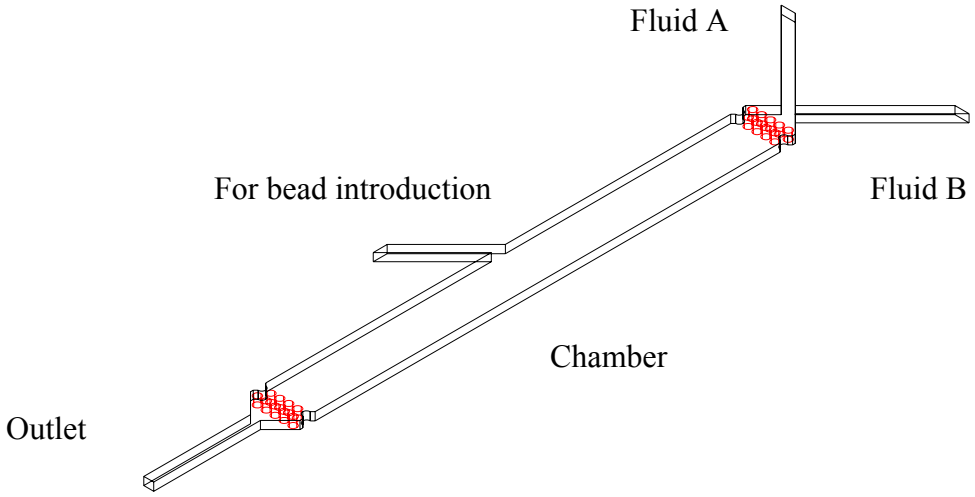

Figure 6-24 Schematic of bead-filled micromixer

6.5 Results and Discussion

In this chapter, the simple Y channel mixer is studied through numerical analysis and experiments. The long mixing channel is needed to give a complete mixing. Implementation of such long mixing channel in a microfluidic device is not practival as it will result in high ashigh pressure drop Interdigital mixer is proposed and investigated The possible improvement is suggested to balance the pressure drop. Finally, porous mixer is proposed and designed.

As mentioned in chapter 2, fluorescent dye is used to quantify mixing. The intensity distribution of fluorescent dye can be measured using Image Pro-Plus software. As demonstrated in Figure 6-7, Figure 6-8 and Figure 6-9, the intensity distribution of fluorescent dye is getting smaller close to the channel. This is caused by the dark contrast of the area outside of the channel as well as the non-uniformity light from the objectives of microscope. Comparing the simulation with the experiments, the concentration or the intensity distribution tends to be uniform as the flow goes downstream. The mixing, however, is not completed.

Even though some improvements are achieved, the proposed interdigital mixers do not work as shown by the simulation. As the strait channel has the same width as the inlet channel, the pressure drop for each inlet channel is determined by both strait channel and inlet channel itself.

Another passive micromixer, porous micromixers is proposed and designed. Using appropriate beads, bead-filled micromixers can be evaluated by experiments.

Chapter 7 Summary and Recommendations

7.1 Contributions of This Thesis

The purpose of this work was to demonstrate and discuss several microfluidic applications and the use of soft lithography for their fabrications. A cell sorting chip with integrated optical elements for detection was evaluated and optimized. Hydroresistance element was implemented in the microfluidic sorting devices to get a reliable hydro-dynamic focusing flow and the effect was investigated. The stable sample flow is very important for accurate detection. For EOF pumping, pressure-driven flow, which is commonly present in microfluidic devices, should be suppressed in order to accurately control the flow. A simple cross channel chip was employed to study the hydoresistance elements and the results can be applied in the experimental chips.

Integrated optical elements for detection were studied through experiments. Reliable optical detection is highly demanded by bio and chemistry analysis. Different integrated optical elements in the microfluidic chip were compared and suggestions for improvement were also proposed. The embedded fiber is simple, but it is impossible to replace the bulky optical system. Hence an integrated optical beamspliter and waveguides in the microfluidic chip were designed and evaluated using the fluorescent beads. Coupler was deployed to couple the light source to the microfluidic chip.

The last part of this work focused on the investigation on micromixers. Active mixers need extra power input which inevitably results in a larger and more complicated system while simple passive mixers need long time to achieve mixing efficiency. Hence a modified interdigital mixer was proposed to overcome the problem.Porous mixer was also proposed and designed but further evaluation should be conducted in lab.

7.2 Recommendations for Future Work

7.2.1 Integrated Optical Elements in the Microfluidic Device

To have a truly portable microfluidic device, further integration of peripheral facilities into the devices is necessary. Integrated beamspliter and waveguide have been investigated and shown to be able to detect the signals from 4um particles. However external features such as laser and fibre are still used and it will be good if they can be embedded in the devices. One possible approach is to use laser diodes to replace lasers. Through aligning laser diodes directly to the coupler, the requirement of a fibre may be eliminated. Furthermore, a reliable and strong bonding process of SU8 to PDMS has to be devised.

7.2.2 Micromixer

In this work, passive mixers were evaluated. The modified interdigital mixer can not work well. Another porous micromixer was recommended and designed. Challenges with porous micromixer include the requirement of appropriate beads, and precise confinement of the beads in the chamber.

References

Beebe, D. J., G. A. Mensing, et al. (2002). "Physics and applications of microfluidics in biology." Annual Review of Biomedical Engineering **4**: 261-286.

Bello, M. S. (1996). "Electrolytic modification of a buffer during a capillary electrophoresis run." Journal of Chromatography A **744**(1-2): 81-91.

Bessoth, F. G., A. J. deMello, et al. (1999). "Microstructure for efficient continuous flow mixing." Analytical Communications **36**(6): 213-215.

Bird, R. B. (1960). "Transport Phemomena." John Wiley & Sons, New York, NY.

Chabinyc, M. L., D. T. Chiu, et al. (2001). "An integrated fluorescence detection system in poly(dimethylsiloxane) for microfluidic applications." Analytical Chemistry **73**(18): 4491-4498.

Chien, F. L. and L. Bousse (2002). "Electroosmotic pumping in microchips with nonhomogeneous distribution of electrolytes." Electrophoresis **23**(12): 1862-1869.

Clayton, J. (2005). "Go with the microflow." Nature Methods **2**(8): 621-627.

Dittrich, P. S. and A. Manz (2006). "Lab-on-a-chip: microfluidics in drug discovery." Nature Reviews Drug Discovery **5**(3): 210-218.

Eckenrode, H. M., S. H. Jen, et al. (2005). "Adsorption of a cationic dye molecule on polystyrene microspheres in colloids: Effect of surface charge and composition probed by second harmonic generation." Journal of Physical Chemistry B **109**(10): 4646-4653.

Elliot, D. J. (1986). "Microlithography: Process Technology for IC Fabrication." McGraw-Hill, New York, NY.

Erickson, D. (2005). "Towards numerical prototyping of labs-on-chip: modeling for integrated microfluidic devices." Microfluidics and Nanofluidics **1**(4): 301-318.

Erickson, D. and D. Q. Li (2004). "Integrated microfluidic devices." Analytica Chimica Acta **507**(1): 11-26.

Fitzgerald, D. A. (2002). "Riding the microfluidic wave." Scientist **16**(23): 40-42.

Fletcher, P. D. I., S. J. Haswell, et al. (2001). "Electrical currents and liquid flow rates in micro-reactors." Lab on a Chip **1**(2): 115-121.

Fluri, K., G. Fitzpatrick, et al. (1996). "Integrated capillary electrophoresis devices with an efficient postcolumn reactor in planar quartz and glass chips." Analytical Chemistry **68**(23): 4285-4290.

Gobby, D., P. Angeli, et al. (2001). "Mixing characteristics of T-type microfluidic mixers." Journal of Micromechanics and Microengineering **11**(2): 126-132.

Greenwald, E. K. (1991). " Electrical Hazards and Accidents: Their Cause and Prevention." Van Nostrand Reinhold, New York, NY.

Hadd, A. G., D. E. Raymond, et al. (1997). "Microchip device for performing enzyme assays." Analytical Chemistry **69**(17): 3407-3412.

Hardt, S. and F. Schonfeld (2003). "Laminar mixing in different interdigital micromixers: II. Numerical simulations." Aiche Journal **49**(3): 578-584.

Hessel, V., S. Hardt, et al. (2003). "Laminar mixing in different interdigital micromixers: I. Experimental characterization." Aiche Journal **49**(3): 566-577.

Hessel, V., H. Lowe, et al. (2005). "Micromixers - a review on passive and active mixing principles." Chemical Engineering Science **60**(8-9): 2479-2501.

Hinsmann, P., J. Frank, et al. (2001). "Design, simulation and application of a new micromixing device for time resolved infrared spectroscopy of chemical reactions in solution." Lab on a Chip **1**(1): 16-21.

Ho, C. M. and Y. C. Tai (1998). "Micro-electro-mechanical-systems (MEMS) and fluid flows." Annual Review of Fluid Mechanics **30**: 579-612.

Huh, D., W. Gu, et al. (2005). "Microfluidics for flow cytometric analysis of cells and particles." Physiological Measurement **26**(3): R73-R98.

Hunter, R. J. (1981). "Zeta Potential in Colloid Science: Principles and Applications." Academic Press, New York, NY.

Jacobson, S. C., T. E. McKnight, et al. (1999). "Microfluidic devices for electrokinetically driven parallel and serial mixing." Analytical Chemistry **71**(20): 4455-4459.

Jean Berthier, P. S., Ed. (2006). Microfluidics for Biotechnology Atech House, Norwooe, MA.

Jorgensen, A. M., K. B. Mogensen, et al. (2003). "A biochemical microdevice with an integrated chemiluminescence detector." Sensors and Actuators B-Chemical **90**(1-3): 15-21.

Kakuta, M., D. A. Jayawickrama, et al. (2003). "Micromixer-based time-resolved NMR: Applications to ubiquitin protein conformation." Analytical Chemistry **75**(4): 956-960.

Kamei, T., B. M. Paegel, et al. (2003). "Integrated hydrogenated amorphous Si photodiode detector for microfluidic bioanalytical devices." Analytical Chemistry **75**(20): 5300-5305.

Kawachi, M. (1996). "Recent progress in silica-based planar lightwave circuits on silicon." Iee Proceedings-Optoelectronics **143**(5): 257-262.

Knight, J. B., A. Vishwanath, et al. (1998). "Hydrodynamic focusing on a silicon chip: Mixing nanoliters in microseconds." Physical Review Letters **80**(17): 3863-3866.

Kuo, J. S., C. L. Kuyper, et al. (2004). "High-power blue/UV light-emitting diodes as excitation sources for sensitive detection." Electrophoresis **25**(21-22): 3796-3804.

Lee, G. B., C. H. Lin, et al. (2003). "Micro flow cytometers with buried SU-8/SOG optical waveguides." Sensors and Actuators a-Physical **103**(1-2): 165-170.

Li, D. (2004). "Electrokinetics in Microfluidics." Elsevier Academic, San Diego, CA.

Li, P. C. H. (2006). "Microfluidic Lab-on-a-Chip for Chemical and Biological Analysis and Discovery." Taylor & Francis Group, Boca Raton, FL.

Lin, C. H., G. L. Chang, et al. (2002). "Micro flow cytometers with buried SU-8/SOG optical waveguides for on-line cell counting." International Journal of Nonlinear Sciences and Numerical Simulation **3**(3-4): 177-180.

Lin, C. H. and G. B. Lee (2003). "Micromachined flow cytometers with embedded etched optic fibers for optical detection." Journal of Micromechanics and Microengineering **13**(3): 447-453.

Liu, R. H., M. A. Stremler, et al. (2000). "Passive mixing in a three-dimensional serpentine microchannel." Journal of Microelectromechanical Systems **9**(2): 190-197.

Masliyah, J. H. (1994). "Electrokinetic Transport Phenomena." AOSTRA, Edmonton, AB.

McDonald, J. C., D. C. Duffy, et al. (2000). "Fabrication of microfluidic systems in poly(dimethylsiloxane)." Electrophoresis **21**(1): 27-40.

Melamed, M. R., Lindmo, T., Mendelsohn, M.L. (1990). " Flow Cytometry and Sorting." 2nd Edition, John Wiley & Sons, New York, NY.

Miyaki, K., Y. L. Guo, et al. (2005). "Fabrication of an integrated PDMS microchip incorporating an LED-induced fluorescence device." Analytical and Bioanalytical Chemistry **382**(3): 810-816.

Nguyen, N.-T. (2006). "Fundamentals and applications of microfluidics." 2^{ed} Artech House,Norwood, MA.

Nguyen, N. T. and Z. G. Wu (2005). "Micromixers - a review." Journal of Micromechanics and Microengineering **15**(2): R1-R16.

Qiao, R. and N. R. Aluru (2002). "A compact model for electroosmotic flows in microfluidic devices." Journal of Micromechanics and Microengineering **12**(5): 625-635.

Quake, S. R. and A. Scherer (2000). "From micro- to nanofabrication with soft materials." Science **290**(5496): 1536-1540.

Recktenwald, D., Radbruch, A. (1998). "Cell Separation Methods and Applications,." Marcel Dekker Inc., New York, NY.

Reyes, D. R., D. Iossifidis, et al. (2002). "Micro total analysis systems. 1. Introduction, theory, and technology." Analytical Chemistry **74**(12): 2623-2636.

Rieseberg, M., C. Kasper, et al. (2001). "Flow cytometry in biotechnology." Applied Microbiology and Biotechnology **56**(3-4): 350-360.

Rolland, J. P., E. C. Hagberg, et al. (2004). "High-resolution soft lithography: Enabling materials for nanotechnologies." Angewandte Chemie-International Edition **43**(43): 5796-5799.

Ruano-Lopez, J. M., M. Aguirregabiria, et al. (2006). "A new SU-8 process to integrate buried waveguides and sealed microchannels for a Lab-on-a-Chip." Sensors and Actuators B-Chemical **114**(1): 542-551.

Ruano, J. M., A. Glidle, et al. (2003). "Design and fabrication of a silica on silicon integrated optical biochip as a fluorescence microarray platform." Biosensors & Bioelectronics **18**(2-3): 175-184.

Shapiro, H. M. (2003). " Practical Flow Cytometry." 4th Edition, John Wiley & Sons, Hoboken, NJ.

Sinton, D. (2003). "Flow Visualization in Microchannels." PhD Thesis, University of Toronto.

Squires, T. M. and S. R. Quake (2005). "Microfluidics: Fluid physics at the nanoliter scale." Reviews of Modern Physics **77**(3): 977-1026.

Stone, H. A., A. D. Stroock, et al. (2004). "Engineering flows in small devices: Microfluidics toward a lab-on-a-chip." Annual Review of Fluid Mechanics **36**: 381-411.

Tabeling, P. (2005). "Introduction to Microfluidics." Oxford University Press, New York, NY.

Taylor, J. (2007). "The Design and Evaluation of a Microfluidic Cell Sorting Chip." Master's thesis, University of Waterloo.

Vassallo, C. (1991). "Optical Waveguide Concepts." Elserier Science, New York, NY.

Vilkner, T., D. Janasek, et al. (2004). "Micro total analysis systems. Recent developments." Analytical Chemistry **76**(12): 3373-3385.

Walker, G. M. and D. J. Beebe (2002). "A passive pumping method for microfluidic devices." Lab on a Chip **2**(3): 131-134.

Wang, H. and W. Li (2007). "A novel 3D porous micromixer fabricated using selective ultrasonic foaming." Journal of Micromechanics and Microengineering **17**(9): 1835-1842.

White, F. M. (1999). "Fluid Mechanics." 4th Edition, McGraw-Hill, New York, NY.

WolfgangEhrfeld, V. H. a. H. L. (2000). "Microreactors." Wiley-VCH.

Wong, S. H., P. Bryant, et al. (2003). "Investigation of mixing in a cross-shaped micromixer with static mixing elements for reaction kinetics studies." Sensors and Actuators B-Chemical **95**(1-3): 414-424.

Wong, S. H., M. C. L. Ward, et al. (2004). "Micro T-mixer as a rapid mixing micromixer." Sensors and Actuators B-Chemical **100**(3): 359-379.

Xia, Y. N. and G. M. Whitesides (1998). "Soft lithography." Annual Review of Materials Science **28**: 153-184.

Xiang, Q., X. C. Xuan, et al. (2005). "Multi-functional particle detection with embedded optical fibers in a poly(dimethylsiloxane) chip." Instrumentation Science & Technology **33**(5): 597-607.

Yang, R. J., C. C. Chang, et al. (2005). "A new focusing model and switching approach for electrokinetic flow inside microchannels." Journal of Micromechanics and Microengineering **15**(11): 2141-2148.

Yang, S. Y., S. K. Hsiung, et al. (2006). "A cell counting/sorting system incorporated with a microfabricated flow cytometer chip." Measurement Science & Technology **17**(7): 2001-2009.

Yi, M. Q. and H. H. Bau (2003). "The kinematics of bend-induced mixing in micro-conduits." International Journal of Heat and Fluid Flow **24**(5): 645-656.